Cortico-cerebellar coordination facilitates neuroprosthetic learning

Aamir Abbasi[1], Andrew W. Fealy[1], Nathan P. Danielsen[1], Tanuj Gulati[1,2,#]

[1] Center for Neural Science and Medicine, Departments of Biomedical Sciences and Neurology, Cedars-Sinai Medical Center, Los Angeles, CA.

[2] Department of Medicine, David Geffen School of Medicine, and Department of Bioengineering, Henry Samueli School of Engineering, University of California-Los Angeles, Los Angeles, CA.

[#] Correspondence: tanuj.gulati@csmc.edu

Abstract

Temporal coordination among neurons and development of functional neuronal assemblies is central to nervous system function and purposeful behavior. Still, there is a paucity of evidence about how functional coordination emerges in neuronal assemblies in cortical and subcortical regions that are directly related to the control of functional output. We investigated emergent neural dynamics between primary motor cortex (M1) and the contralateral cerebellar cortex as rats learned a neuroprosthetic/ brain-machine interface (BMI) task. BMIs offer a powerful tool to causally test how distributed neural networks achieve specific neural patterns. During neuroprosthetic learning, actuator movements are causally linked to primary motor cortex (M1) neurons, i.e., “direct” neurons, that project to the decoder and whose firing is required to successfully perform the task. However, it is unknown how such direct M1 activity interacts with cerebellar activity. We observed a striking 3-6 Hz coherence that emerged between these regions’ local-field potentials (LFPs) with neuroprosthetic learning which also modulated task-related spiking. We found a robust task-related indirect modulation in the cerebellum, and we found that it became synchronous with M1-direct activity with learning. We also performed optogenetic inhibition of cerebellar activity and found that this led to performance impairments in neuroprosthetic control. Together, these results demonstrate that coordinated neural dynamics emerge in cortico-cerebellar regions during neuroprosthetic learning which supports task-relevant activity in M1 direct neuronal populations, and further, that cerebellar influence is necessary for M1-driven rapid direct neural control.

Keywords: Cerebellum, motor cortex, brain-machine interface

Introduction

To accomplish even the simplest of tasks, the nervous system coordinates activity across distant brain regions. For example, holding a bottle full of water requires several neurons to produce well-calibrated muscle forces for grasping and monitoring sensory feedback. Parallel processes in several sensorimotor regions underlie even the most trivial tasks such as above. Dense reciprocal connectivity between these regions supports this processing which likely need to be configured rapidly and flexibly to support a repertoire of behavior and afford learning of new skills. Two motor regions, the primary motor cortex (M1) and the cerebellum, have dense reciprocal connections, and are known to be involved in motor learning[1,2]. Studies have shown how learning alters local activity in the cerebellum or M1[3–6], yet learning also alters task-related cross area coordination[2,7]. Both M1 and the cerebellum have dense connections with other cortical and subcortical regions, and hence it is difficult to ascertain if changes in interaction are because of direct interactions between M1 and cerebellum[8–10], or because of their roles coordinating the upper limb.

To isolate the effects of M1 and cerebellum to movement control versus the direct task-related coordination, we have used a brain-machine interface task, where select M1 neurons (*'direct'* neurons) modulate their activity to control an external disembodied actuator. This offers experimenters a powerful paradigm where they can dictate/set the neuron-behavior relationship. During "brain control", direct M1 neurons change their firing properties during neuroprosthetic learning[11–18]. In addition, other neurons in the local M1 network also become task-coupled (i.e., *'indirect'* neurons)[12,13,15,19–23]. It remains

68 unknown what activity emerges in the cerebellum with M1-driven neuroprosthetic learning
69 and what role it plays. Here, we hypothesized that cerebellum neurons will demonstrate
70 task-related firing during M1-driven neuroprosthetic learning. We also predicted that
71 modulating the cerebellum optogenetically will impact M1-driven neuroprosthetic
72 learning.
73
74 Another focus of our investigations was on co-emergent synchronous activity across M1
75 and cerebellum with neuroprosthetic learning. Recent theories have proposed that
76 alterations in the pattern of synchronous activity across regions can serve to coordinate
77 network activity for natural and neuroprosthetic behaviors[20,24]. Such transient local-field
78 potential (LFP) activity can modulate excitability of cell groups across varying
79 spatiotemporal scales[25,26]. This helps in achieving precise temporal control in neural
80 networks that can enhance information transfer in specific cell populations[27] and can
81 influence spike-timing-dependent plasticity[28]. Such temporally coordinated activity among
82 ensembles underlies diverse neural processes ranging from perception, decision making,
83 action, memory and attention[6,29–33]. Importantly, spiking in one region becomes
84 coordinated with LFP in another region, indicative of synchrony[30,34]. Despite the evidence
85 that synchronous LFP is related to learning[6,35], there is a paucity of evidence that this
86 selectively modulates task-relevant activity of neurons across brain areas. Using the
87 neuroprosthetic task paradigm, where we can control the neurons that are linked to
88 behavioral output, we aimed to disentangle the synchronous activity of “direct” neurons
89 within M1 locally and with task-relevant indirect activity in the cerebellum to understand
90 how these diverse classes of cells were modulated by synchronous LFP.

We have used a BMI paradigm in which a small set of M1-direct neurons controlled a simple 1-D actuator[12,18,21]. We recorded additional neural activity from neighboring indirect neurons in M1, as well as distant cerebellar cortex. First, we found that cerebellar neurons developed strong 'task-related' indirect modulation, and M1 and cerebellum developed a 3-6Hz LFP coherence with neuroprosthetic learning. We also found that direct M1 neurons and task-related indirect neurons in both M1 and cerebellum enhanced their phase-locking to this 3-6Hz oscillation in the LFPs. Next, we also found that synchronous spiking between M1 direct neurons and cerebellar indirect neurons increased with neuroprosthetic learning, and fine timescale coordination between these regions also increased as evaluated through canonical correlation analyses. In our last set of experiments, we optogenetically inhibited the cerebellum and found that this led to performance impairments in the neuroprosthetic task and weakening of M1-direct activity. Together, our results support a necessary role of cross-area interactions between M1 and cerebellum that underlie neuroprosthetic skill learning.

108 **Results**

109 We implanted microwire electrode arrays in the primary motor cortex (M1) and silicon
110 probes in a tetrode/ polytrode configuration in the cerebellar posterior lobes (see Methods
111 for details). After neural implant surgery, we trained 8 animals to exert direct neural control
112 on the angular velocity of a mechanical actuator that can also deliver water. A linear
113 decoder with randomized weights typically converted the firing rates of two groups of units
114 in M1 (randomly selected and assigned positive or negative weights; hereafter referred
115 to as *'direct'* units; M1 TR_d's) into the angular velocity of the actuator. We also recorded
116 multiple other units in both M1 and cerebellum that were not causally linked to actuator
117 movements but showed task-related modulation (hereafter referred to as *'indirect'* units).
118 The decoder weights were held constant during the session to exclusively rely on neural
119 learning mechanisms. Each trial started with the simultaneous delivery of an auditory tone
120 and opening of a door to allow access to the tube (**Fig. 1 a,b**). At the start of each trial,
121 the angular position of the tube was set to resting position, P_1. If the angular position of
122 the tube was held for >400 ms at target position P_2, a defined amount of water was
123 delivered (that is, successful trial). A trial was stopped if this was not achieved within 15s
124 (that is, unsuccessful trial). At the end of a trial, the actuator was returned to position P_1
125 and the door was closed.

126

127 ***Direct control of BMI by M1 units***

128 We observed that over the course of a typical 1-2h practice session, animals showed
129 improvements in task performance with a significant reduction in the time to successful

trial completion and decrease in the proportion of unsuccessful trials. We report results here from 23 sessions, where we saw significant reductions in both metrics.

Overall we observed that rats showed improvement in task-performance with a significant reduction in the time to a successful trial completion (**Fig. 1c,d**; 7.69 ± 0.42 sec to 4.09 ± 0.3 sec, mixed-effects model: $t(44) = -7.13$, $P = 7.3 \times 10^{-9}$) and a decrease in the percentage of unsuccessful trials (**Fig. 1d**; 28.12 ± 3.65 % to 2.71 ± 0.97 %, mixed-effects model: $t(44) = -7.01$, $P = 1.0 \times 10^{-8}$).

In a subset of sessions, we performed video recording of rats during the BMI training and quantified the proficiency of brain control by ruling out movement of the implanted limb. Consistent with previous reports of lack of muscle contractions during neuroprosthetic control, we did not observe limb movements to systematically predict feeding tube movements[15]. Specifically, we analyzed whether limb movements measured using the video recording correlated with movements of the feeding tube. Across multiple sessions we observed significant reduction of this correlation (**Supplementary Fig 3a,b**; 0.014 ± 0.002 to 0.006 ± 0.001, mixed-effects model: $t(26) = -3.52$, $P = 1 \times 10^{-3}$).

We also analyzed the proportion of TR_d's that developed robust task-related modulation (see Methods). **Figure 1e**, depicts the increase in the activity of M1 direct units from early to late trials. Since the direct units were causally linked to the movement of the actuator, we found that a high proportion of these units developed task-related modulation (96% of 50 TR_d's), as has been reported in the past[11].

153 ***Indirect modulation of neurons in M1 and cerebellum***

154 We also analyzed indirect units in the M1 and cerebellum and checked for their task-
155 related modulation. We further sub-classified indirect units as either task-related (TR_i's)
156 or task-unrelated (*TU's*) based on changes in modulation depth with learning. Consistent
157 with previous reports of indirect units in the M1 likely contributing to neuroprosthetic
158 control[11,13,15,19,21], we found strong indirect modulation in M1 (**Fig. 1f**). Additionally, we
159 found robust indirect modulation of units in the cerebellum (**Fig. 1h**). Majority of units in
160 M1 and cerebellum developed strong indirect task-related modulation with learning (**Fig.**
161 **1j**). We also looked at the change in modulation depth (MD_Δ) and found that M1 TR_d
162 undergoes greater MD_Δ from early to late trials as compared to M1 and Cb TR_i units (M1
163 TR_d : 130.46 ± 47.8%; M1 TR_i : 51.075 ± 15.5%; cerebellum TR_i : 25.88 ± 9.5 %, Kruskal-
164 Wallis H-test, $F_{2,713}$ = 195.23, P = 4.0 x 10^{-43}, *post hoc t*-test showed significant difference
165 among M1 TR_d, TR_i and cerebellum TR_i MD_Δ *'s;* P < 0.05). Our next analyses focused
166 on these task-related cells.

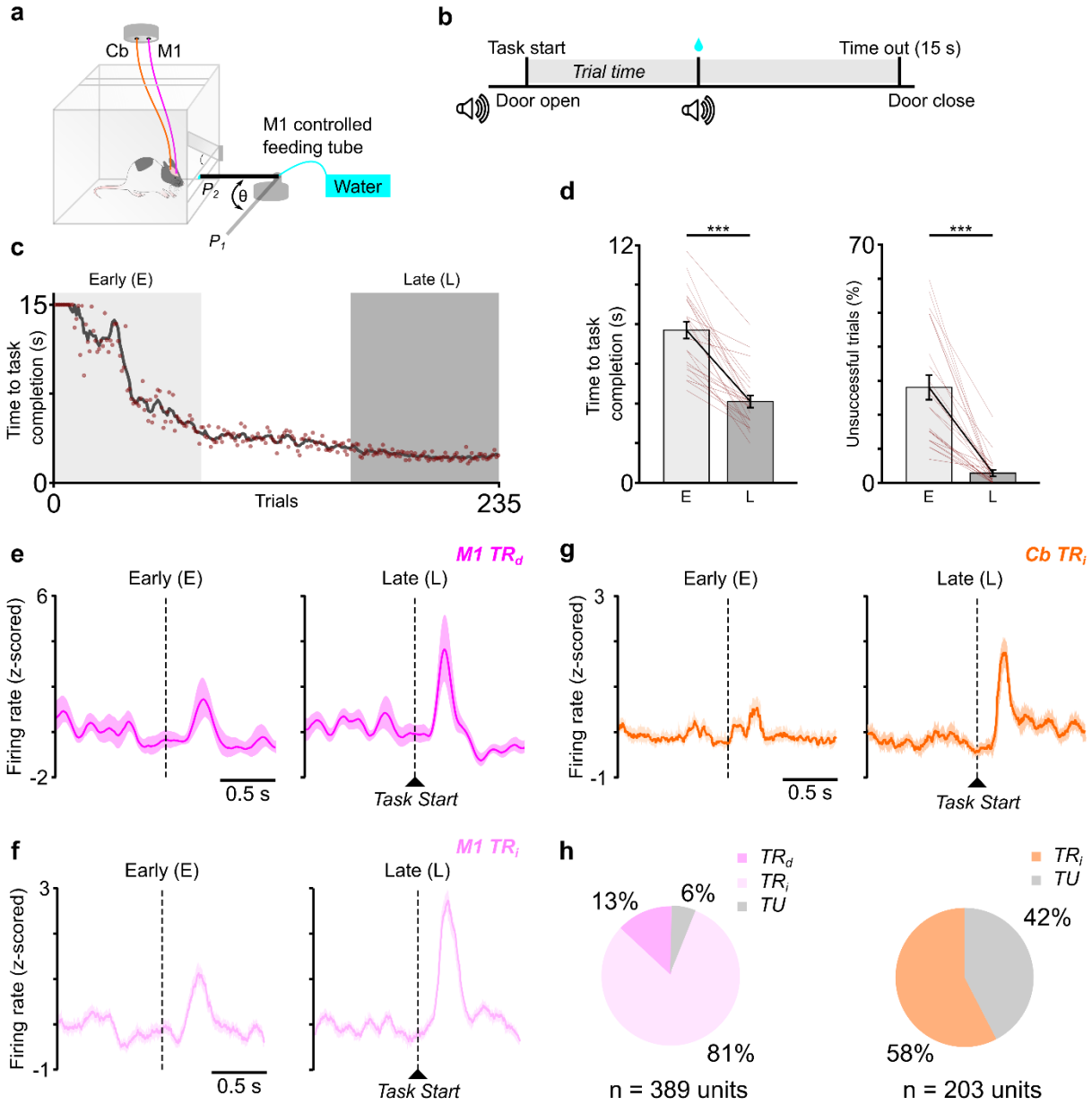

Figure 1. Direct and indirect modulation of M1 and cerebellar activity with neuroprosthetic learning. ***a,*** Direct neural control of a feeding tube (θ = angular position). Each trial started with the tube at P_1. ***b,*** Trial started with an audio tone cue and opening of the door. A successful trial required movement of the tube to P_2 within 15 seconds. ***c,*** Change in task completion time as a function of trial number. Line shows moving average of 5 trials. Dots show raw task completion times across all trials. ***d,*** Change in time to trial completion (*left*) and reduction in the percentage of unsuccessful trials (*right*) from *early* to *late* trials across all sessions. ***e,*** Peri-event histogram (PETH) from *early* and *late* trials from a single session are shown in *left* and *right* panels respectively, M1 TR_d task-related direct units. ***f,*** M1 TR_i units. ***g,*** Cerebellum TR_i units ***h,*** Distribution of units classified as TR_d, TR_i and *TU* in M1 (*top*) and cerebellum (*bottom*). ***p<0.001.

179 ***Emergence of coordinated task-related activity in M1 and cerebellar LFPs***

180 Interestingly, as the rats became proficient in M1-driven neuroprosthetic control, we
181 observed that a coordinated low-frequency activity (approximately 3–6 Hz, **Fig. 2a**)
182 emerged with learning in both M1 and cerebellum. The task-related LFP power between
183 3–6 Hz increased from early to late trials in both M1 (**Fig. 2b,c**; 0.44 ± 0.07 to 0.80 ± 0.075,
184 mixed-effects model: $t(44) = 4.9$, $P = 1.0 \times 10^{-5}$) and the cerebellum (**Fig. 2d,e**; 0.18 ± 0.03
185 to 0.37 ± 0.04, mixed-effects model: $t(44) = 2.5$, $P = 1.0 \times 10^{-2}$). Task-related LFP
186 coherence also increased in the 3−6 Hz frequency range from early to late trials (**Fig. 2f,**
187 **g**; 0.16 ± 0.01 to 0.22 ± 0.013, mixed-effects model: $t(44) = 4.6$, $P = 2.5 \times 10^{-5}$). This
188 emergence of cross-region low-frequency activity is consistent with other observations of
189 emergence of low-frequency activity during motor skill learning across reciprocally
190 connected neural networks[7].

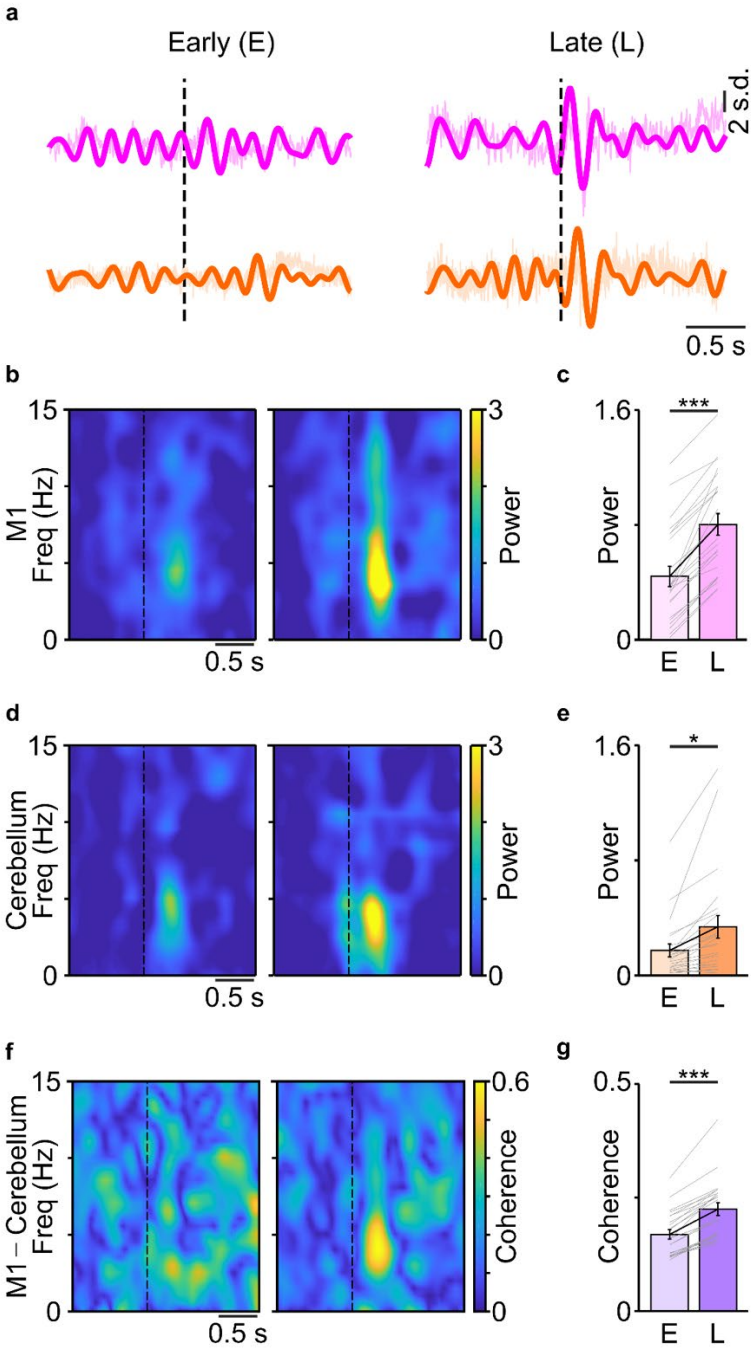

Figure 2. Co-ordinated task-related oscillations emerge in M1 and cerebellar LFPs *a,* Raw and filtered LFP trace from a representative trials showing increase in 3–6 Hz oscillations after task-start during *late* trials in both M1 and cerebellum. ***b,*** Spectrogram from a representative M1 channel showing increase in 3–6 Hz power during *late* trials. **c,** Increase in 3–6 Hz power in M1 LFP from *early* to *late* trials across sessions. ***d,*** Same as ***b*** but from a representative cerebellum LFP channel. ***e,*** Same as ***c*** for 3–6 Hz cerebellum LFP power across sessions. ***f,*** Coherogram from a representative pair of M1–cerebellum LFP channel showing increase in 3–6 Hz coherence during *late* trials. ***g,*** Change in 3–6 Hz coherence from *early* to *late* trials across sessions. *p<0.05, ***p<0.001.

201 ***Increase in locking between spiking and LFP after neuroprosthetic learning***

202 We next investigated the relationship between spiking activity and the low frequency LFP
203 oscillations that we observed during robust task engagement. We performed spike-
204 triggered averaging (STA) of the LFP in *early* and *late* learning time-locked to spikes
205 occurring either in the same region (*i.e.,* M1 spikes to M1 LFP and cerebellum spikes to
206 cerebellum LFP) or in the other region (*i.e.,* M1 spikes to cerebellum LFP and cerebellum
207 spikes to M1 LFP). If spiking activity was independent of low-frequency LFP activity, then
208 fluctuations would cancel and produce a flat average LFP, and hence, the STA can
209 provide an intuitive estimate of how neural spiking is modulated by the low-frequency LFP
210 oscillations. We observed a clear increase in the amplitude of mean LFP oscillations in
211 both regions around action potentials of M1 TR_d, TR_i and cerebellum TR_i units (**Fig. 3a**).
212 This increase was not present for these classes of cells when we did the STA analysis
213 during task-unrelated inter-trial interval (**Fig. 3b**). M1 TR_d and TR_i units, and cerebellum
214 TR_i units experienced 86.15 ± 11.50%, 90.97 ± 3.78% and 83.28 ± 5.95% increases in
215 STA amplitude with M1 LFP during task periods, respectively. During inter-trial interval
216 these units experience a decrease of −3.52 ± 2.68%, −0.25 ± 2.55% and −2.02 ± 2.39%,
217 respectively (**Fig. 3c**; Kruskal-Wallis H-test, $F_{5,137} = 73.74$, $P = 3.0 \times 10^{-20}$, *post hoc t*-test
218 showed significant difference for M1 TR_d, TR_i and cerebellum TR_i during task-relevant
219 period and inter-trial period; $P < 0.001$). When STA was performed with cerebellum LFP,
220 M1 TR_d and TR_i units, and cerebellum TR_i units experienced 80.87 ± 11.28%, 78.52 ±
221 6.83% and 113.75 ± 22.10% increases in STA amplitude (during the task period),
222 respectively. Similar to M1 LFP, these units experienced significantly less change of 2.55
223 ± 1.73%, −0.81 ± 2.85% and 1.44 ± 3.52%, respectively, when STA was performed with

224 cerebellum LFP during inter-trial interval (**Fig. 3d**; Kruskal-Wallis H-test, $F_{5,137}$ = 23.63, P

225 = 5.6 x 10^{-21}, *post hoc t*-test showed significant difference for M1 TR_d, TR_i and cerebellum

226 TR_i during task-relevant period and inter-trial periods; P < 0.001).

227

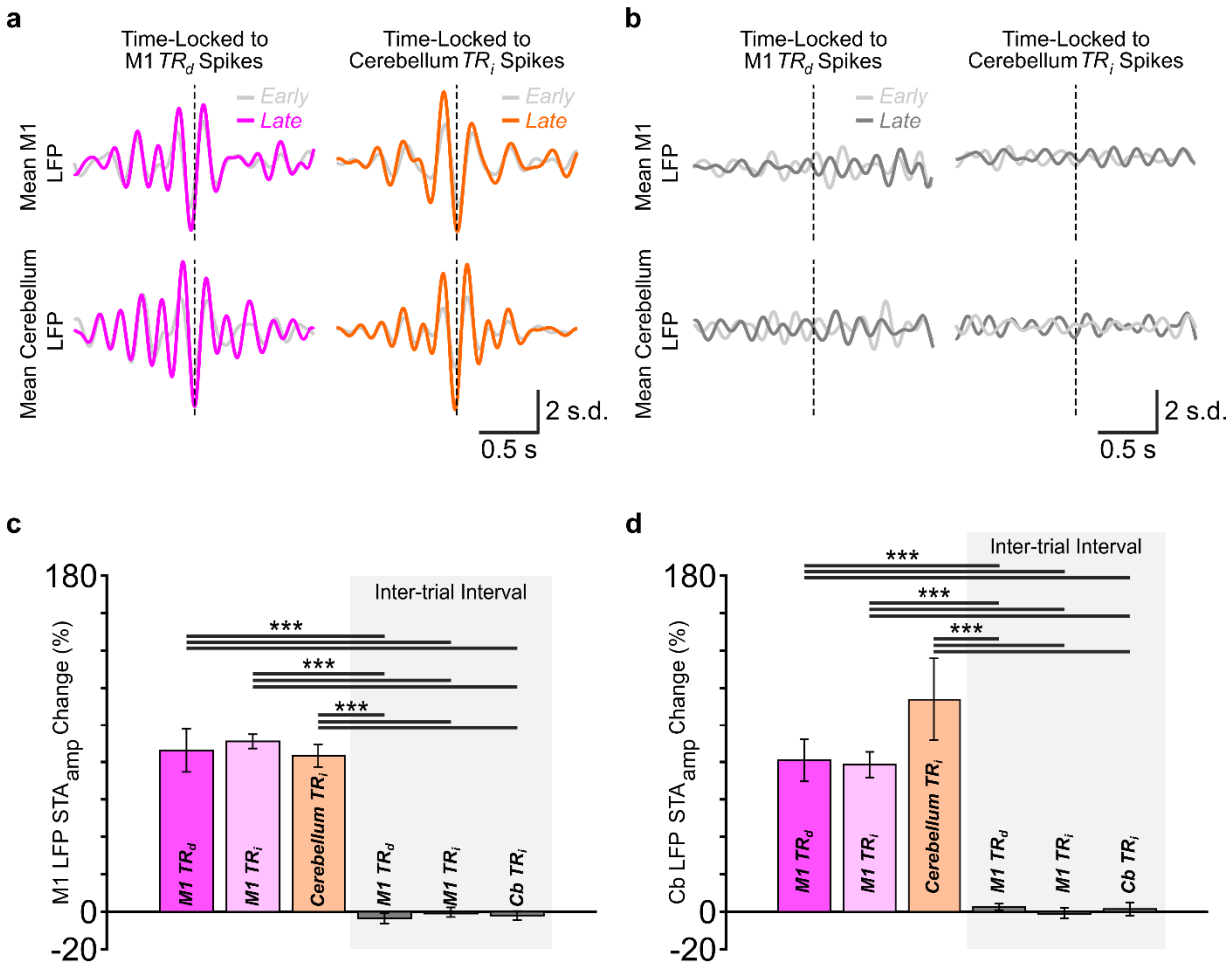

228

229 **Figure 3. M1 and cerebellum spike-LFP locking increases with learning.** ***a,*** The mean M1
230 LFP (*top* row) or cerebellum LFP (*bottom* row) time locked to occurrences of spikes from M1 (left
231 column) or cerebellum (right column) during task-period from a representative session. ***b,*** Same
232 as ***a*** during inter-trial interval. ***c,*** Percentage change in STA amplitude for M1 LFP in each of the
233 categories of units (mean ± s.e.m.). ***d,*** Same as ***c*** for STA of cerebellum LFP. ***p<0.001.
234

235

236

237 ***Increase in neural synchrony between M1 and cerebellum***

238 We subsequently assessed whether there are changes in the correlated spiking among
239 the recorded M1 and cerebellum neural ensembles with neuroprosthetic learning. To
240 analyze this, we looked at how the magnitude of cross-correlation between pairs of M1
241 TR_d 's and cerebellum TR_i 's changed. An example of an increase in cross-correlation is
242 shown in **Fig. 4a**. At the population level, we calculated the magnitude of the difference
243 between the peak average early trials and late trials correlogram from a shuffled
244 correlogram (*ΔCCH*, see "Methods"). We found a significant increase in correlated firing
245 (calculated as an increase in above-mentioned difference) during late trials (**Fig. 4b**;
246 4.52 ± 0.46 to 6.30 ± 0.60, mixed-effects model: $t(44) = 5.15$, $P = 5.8 \times 10^{-6}$). Thus, our
247 findings show that *'direct'* units in M1 (M1 TR_d 's) and *'indirect'* cerebellar TR_i 's fire more
248 coincidently with neuroprosthetic learning.

249

250 We also performed cross-correlation between M1 TR_d 's and M1 TR_i 's. Consistent with
251 previous reports[11,15], we found a significant increase in the magnitude of cross-correlation
252 (**Fig. 4c**; 2.86 ± 0.41 to 4.18 ± 0.46, mixed-effects model: $t(44) = 2.64$, $P = 0.01$). We also
253 performed cross-correlation between M1 TR_i 's and cerebellum TR_i 's (see **Fig. 4d**).
254 Surprisingly, we found no significant change in the magnitude of cross-correlation in this
255 pair with learning (**Fig. 4e**; 3.56 ± 0.69 to 3.11 ± 0.54, mixed-effects model: $t(44) = -1.92$,
256 $P = 0.06$).

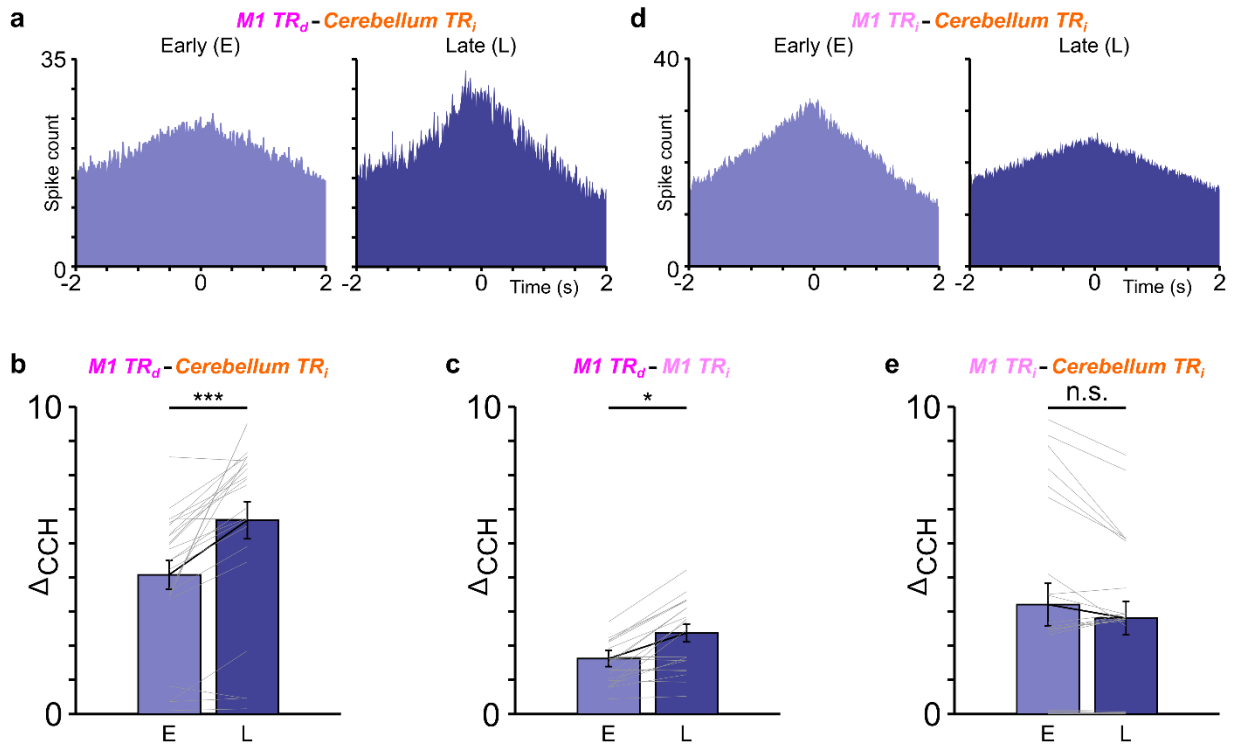

Figure 4. M1 *TR_d* and cerebellar *TR_i* neural synchrony increases with learning. *a,* Representative cross-correlogram of a pair of M1 *TR_d* and cerebellum *TR_i* unit in early (*left*) and late (*right*) trials. ***b,*** Change in magnitude of cross-correlogram from early to late trials across all sessions for all M1 *TR_d* and cerebellum *TR_i* units (mean ± s.e.m.). ***c,*** Same as ***b*** for M1 *TR_d* and M1 *TR_i* units pairs. ***d,*** Representative cross-correlogram of a pair of M1 *TR_i* and cerebellum *TR_i* unit in early (*left*) and late (*right*) trials. ***e,*** Same as ***b*** for M1 *TR_i* and cerebellum *TR_i* unit pairs. *p<0.05 ***p<0.001

Fine timescale coordination of M1 and cerebellum activity with task learning

While our analyses so far show a coordinated activity in M1 and cerebellum with task learning; it doesn't necessarily indicate that the neural activity patterns in the two structures are coordinated across trials. Recent studies have explored fine-timescale coordination at the level of spiking[36,37]. Such methods use statistical methods to measure 'communication subspaces' based on ensemble patterns. Here, we used canonical correlation analysis (CCA) to assess fine-timescale coordination between M1 and cerebellum. CCA has been used in various neuroscience studies to extract correlated

population activity between two areas[36–40]. Specifically, CCA finds a linear combination of units in M1 and cerebellum that project to M1 and cerebellum subspaces, respectively, and where activity in these subspaces is maximally correlated (**Fig. 5a**). We used concatenated single-trial spiking activity binned at 100ms as in two recent papers[37,40]. The top component produced by CCA is the axis of the M1 and cerebellar subspaces that has the maximum correlation between the two areas. We found that this maximum correlation increased with neuroprosthetic learning only for M1 TR_d and cerebellum TR_i units (**Fig. 5b** shows CCA changes in an example session from a single animal, and **Fig. 5c** shows all sessions from all animals; *early* canonical correlation: 0.24 ± 0.032, *late* canonical correlation 0.54 ± 0.035, mixed-effects model: $t(44) = 7.55$, $P = 1.7 \times 10^{-9}$). Moreover, we found that the subspace activity in the two structures became more precisely temporally correlated with learning (**Fig. 5d)**. For M1 TR_i 's and cerebellar TR_i 's, maximal correlation produced by CCA didn't show a significant increase (**Supplementary Fig. 4**; 0.37 ± 0.042 to 0.39 ± 0.045, mixed-effects model: $t(44) = 0.52$, $P = 0.604$).

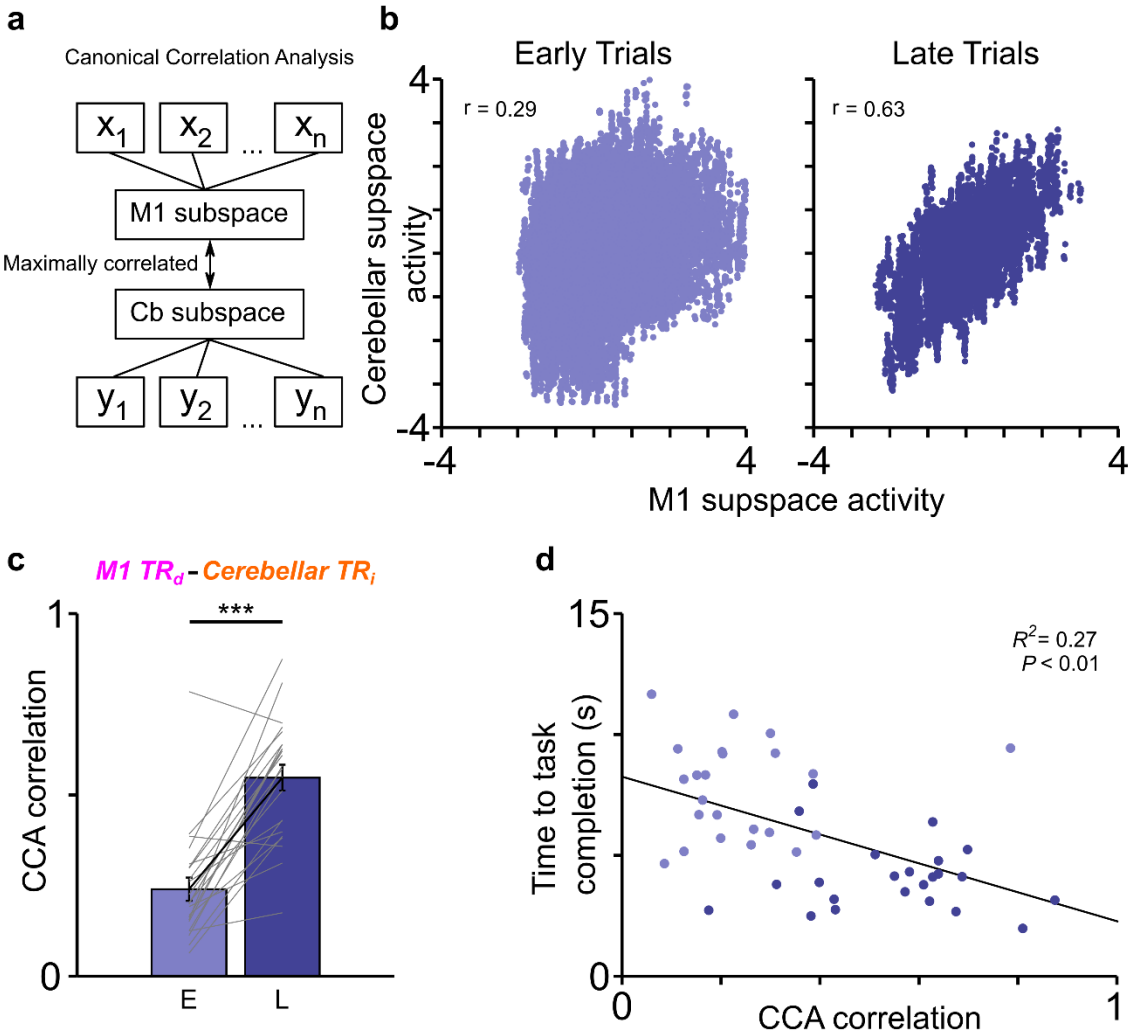

Figure 5. Increase in neural subspace correlation between M1 and cerebellum. ***a,*** Description of canonical correlation analysis (CCA). CCA finds a linear combination of binned spike counts from M1 units (x_1, x_2, … x_n) and cerebellum units (y_1, y_2, …, y_n) that maximizes the correlation between M1 and cerebellum. ***b,*** M1 TR_d and cerebellum TR_i subspace activity (from the first canonical component) around task-start (−2 to 2 s) for an example session. Each dot represents one time bin of *early* or *late* trials from the session. Canonical correlation score is given by *r*. ***c,*** Change in the canonical correlation score from *early* to *late* trials across all sessions. ***p<0.001. ***d,*** Relationship between CCA correlation score and average time to a succesful trial across all sessions.

307 ***Cerebellar indirect modulation leads M1 response after task onset***

308 With recent reports of M1 activity being input driven and secondary motor cortex's (M2)
309 modulatory influence over M1 during M1-driven neuroprosthetic task[37,41], we wanted to
310 check how did the cerebellar TR_i activity 'integrate' with M1 TR_d activity. Interestingly,
311 both early and late in learning, the temporal profiles of modulation (i.e., **Fig. 6a)** for M1
312 TR_d and cerebellar TR_i were different, suggesting that these two distinct groups of task-
313 related units became functionally and temporally coupled with learning and successful
314 task performance. Additionally, we also observed that cerebellum TR_i activity tended to
315 peak before M1 TR_d during early trials (**Fig. 6b**; time to peak for M1 activity:
316 252.27 ± 15.53 ms and time to peak for cerebellum activity: 228.08 ± 14.18 ms, mixed-
317 effects model: $t(332) = -1.20$, $P = 0.23$) and late trials (**Fig. 6c**; time to peak for M1
318 activity: 249.92 ± 5.99 ms and time to peak for cerebellum activity: 231.51 ± 5.86 ms,
319 mixed-effects model: $t(332) = -2.19$, $P = 0.02$).

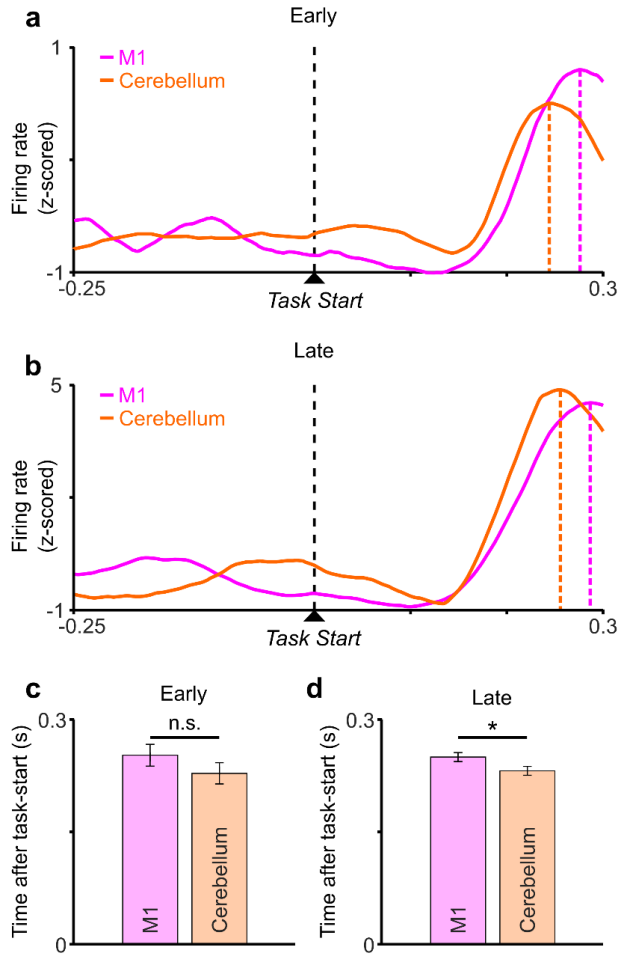

Figure 6. Cerebellum TR_i activity peaks before M1. ***a,*** PETH showing the difference of time-to-peak for a M1 TR_d and cerebellum TR_i units during early trials. ***b,*** Same as ***a*** for late trials. ***c,*** Difference between time to peak across all M1 TR_d and cerebellum TR_d units during *early* trials. ***d,*** Same as ***c*** for *late* trials. n.s. indicates p>0.05 *p<0.05.

Cerebellar optogenetic inhibition impairs neuroprosthetic performance

Next, we wanted to see the effects of optogenetic inhibition of cerebellum and the effects on neuroprosthetic skill learning. We used a red-light shifted halorhodopsin- JAWS for inhibiting neural activity in the cerebellum (see Methods). First, we found that JAWS was robustly expressed in cerebellar cortical neurons **(Fig. 7a**). When we looked at the activity of cerebellar neurons under optical illumination acutely, we found that JAWS activation

333 led to strong inhibition of cerebellar neurons (**Supplementary Fig. 5a,b**). Optogenetic
334 inhibition significantly reduced firing across cerebellar neurons (**Supplementary Fig. 5c**;
335 $Stim_{pre}$: 27.30 ± 2.88 Hz, $Stim_{ON}$: 4.99 ± 0.67 Hz and $Stim_{post}$: 20.16 ± 2.09 Hz; $Stim_{pre}$ vs
336 $Stim_{ON}$ mixed-effects model: $t(88) = -7.69$, $P = 1.9 \times 10^{-11}$; $Stim_{post}$ vs $Stim_{ON}$ mixed-
337 effects model: $t(88) = 7.05$, $P = 3.8 \times 10^{-10}$) , with a reduction in 84.44% of recorded cells
338 during $Stim_{ON}$: (n = 45).
339
340 Next, we performed optogenetic inhibition of the cerebellum in chronically implanted rats
341 during the BMI task practice (see Methods). When we inhibited the cerebellum in rats that
342 had already gained proficiency in neuroprosthetic task performance (*i.e.,* during *late*
343 trials), we found that time to successful completion of neuroprosthetic task increased (**Fig.
344 7b**; 5.95 ± 0.68s without cerebellum inhibition and 8.85 ± 0.69 s with cerebellum inhibition,
345 mixed-effects model: $t(22) = 3.24$, $P = 3.7 \times 10^{-3}$). Furthermore, we also found that
346 cerebellar inhibition decreased the MD_{Δ} of M1 TR_d units during trials when cerebellum
347 was optogenetically inhibited (**Fig. 7c,d**; 190.11 ± 49.86% without cerebellum inhibition
348 and 112.11 ± 17.42% with cerebellum inhibition, mixed-effects model: $t(34) = -1.71$,
349 $P = 1 \times 10^{-2}$). Interestingly, this effect of cerebellar inhibition was not as strong on M1 TR_i
350 units as it was on M1 TR_d units (**Supplementary Fig. 6**; MD_{Δ} for M1 TR_i units:
351 48.67 ± 6.90% without cerebellum inhibition and 47.13 ± 4.77% with cerebellum inhibition,
352 mixed-effects model: $t(391) = -0.15$, $P = 0.87$). Cerebellar inhibition also impacted M1
353 3−6 Hz LFP power. During late trials, 3−6 Hz M1 power was reduced under cerebellar
354 inhibition (**Fig. 7e,f**; 1.29 ± 0.14 z-scored M1 power without cerebellum inhibition and

355 0.73 ± 0.11 M1 power with cerebellum inhibition, mixed-effects model: $t(22) = -3.30$,
356 $P = 3.2 \times 10^{-3}$).
357
358 While these experiments spoke about loss of performance on the neuroprosthetic task
359 when cerebellum was optogenetically inhibited, we also observed that the effects of
360 cerebellar inhibition on neuroprosthetic learning was not related to the order in which it
361 was performed, i.e., effects of inhibition of cerebellum in first BMI block versus the second
362 BMI block within a day with the same M1 TR_d units (see Methods for details on the order
363 of two BMI blocks within a day), **Supplementary Fig. 7b**; time to task completion with
364 cerebellum inhibition in first BMI block: 9.33 ± 0.86s versus time to task completion
365 without cerebellum inhibition in second BMI block: 6.34 ± 1.02s, mixed-effects model:
366 $t(12) = -2.58$, $P = 2 \times 10^{-2}$. **Supplementary Fig. 7c**; Time to task completion without
367 cerebellum inhibition in first BMI block: 5.54 ± 0.9s versus time to task completion with
368 cerebellum inhibition in second BMI block: 7.98 ± 1.49s, mixed-effects model: $t(8) = 1.74$,
369 $P = 1 \times 10^{-2}$). Hence, our results show that cerebellum was actively involved in supporting
370 rapid M1-driven neuroprosthetic control, whether the animals were new to the BMI control
371 scheme or when they had become proficient with a given control scheme.
372

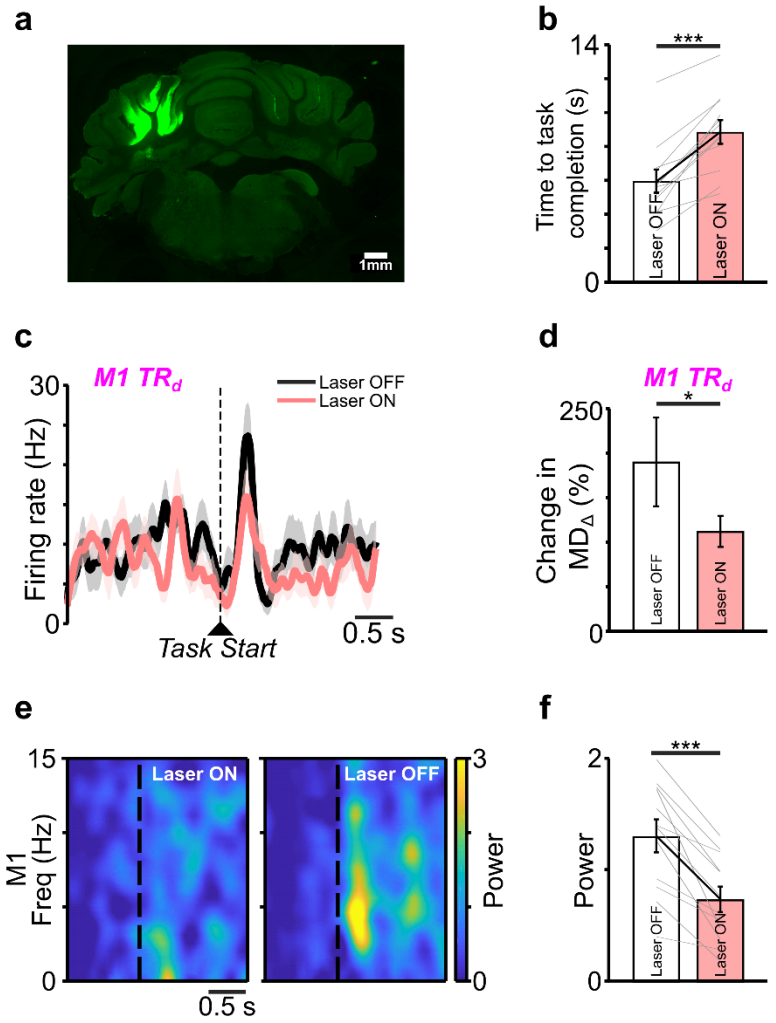

Figure 7. BMI performance gets impaired with cerebellar inhibition *a*, Fluorescence image of a coronal brain section showing neurons expressing JAWS (green) in the cerebellum cortex. ***b*,** Cerebellar inhibition increases time to task completion. ***p<0.001. ***c*,** PETH of an example M1 TR_d unit, during *late* trials, with (Laser ON) and without (Laser OFF) cerebellar inhibition. ***d*,** Change in modulation depth (MD_Δ) of M1 TR_d units from *early* to *late* trials, with and without cerebellar inhibition. *p<0.05. ***e*,** Spectrograms of an example M1 LFP channel showing an absense of 3-6 Hz power during cerebellar inhibition (left) in *late* trials. The 3-6 Hz power emerges during *late* trials in the same day session where cerebellar inhibition was not done. ***f*,** The 3-6 Hz power emerges during *late* trials on the same day session where cerebellar inhibition was not done.

385 **Discussion**

386 In this study, we found an emergent 3-6Hz activity in the M1 and cerebellum LFPs that
387 also modulated task-related direct and indirect spiking in these regions. Additionally, we
388 found that neuroprosthetic learning led to increased synchronous spiking between M1
389 TR_d and cerebellar TR_i units, and this pair also had a stronger spiking coordination across
390 trials as indicated by heightened canonical correlation with learning. Furthermore,
391 optogenetic inhibition of the cerebellum led to performance impairments (with increased
392 time to task completion) and weakening of M1 TR_d activity. At population spiking level,
393 we also found that cerebellar activity was leading M1 direct activity. These findings
394 suggest that cerebellum plays an important hierarchical role by providing influence on M1
395 neural patterns that are related to behavioral output. Furthermore, we found that
396 cerebellar indirect activity became more synchronous with M1 direct activity and
397 canonical correlation also increased between M1 TR_d and cerebellum TR_i 's, but this was
398 not observed for M1 TR_i and cerebellum TR_i units suggesting that cerebellum had a more
399 privileged relationship with effector-specific neurons of M1. Although we found that M1
400 TR_i*'s* correlated activity increased with M1 TR_d units, indicating that same-area
401 interactions also participate in achieving neuroprosthetic skill learning, cerebellum TR_i*'s*
402 preferential coordinated activity with only M1 direct units suggests that cerebellum has a
403 strong selective online modulatory influence on M1, as well as instantiating behaviorally
404 relevant patterns. This role of cerebellum that we found in neuroprosthetic skill learning
405 is consistent with cerebellum's role in fine-tuning movement, as well as co-emergent
406 activity patterns that have been reported with learning new skills[2,42]. Our studies here
407 have helped elucidate cerebellar contributions to M1-driven neuroprosthetic learning and

408 can help improve BMI functionality in the future. For example, BMI paradigms could
409 incorporate cerebellar indirect signals for improving BMI controllers.
410
411 ***Emergent mesoscopic dynamics across M1-cerebellum***
412 One of our first findings was an emergence of 3-6 Hz coherence in M1- cerebellum LFPs
413 associated with learning, and neurons in both these regions also showed enhanced
414 phase-locking to this oscillation during task-relevant periods as revealed through STA.
415 Similar observations have been observed in a neuroprosthetic study that looked at task-
416 related cells in cortico-striatal networks[20]. Such coherence can serve to enhance
417 communication during task period between task-relevant cell populations across the
418 larger motor networks that should integrate signals for optimal behavioral output. Such
419 coherent activity may allow for flexible use of task-relevant cells in either region. The
420 synchrony that we observed in 3-6 Hz band is consistent with other work that has showed
421 low-frequency coherence between M1 and other motor regions during learning[6,7].
422
423
424 ***Using BMIs to study cross-region coordination in motor control.***
425 BMI offers investigations of connected regions by selecting target neural patterns (that
426 dictate output) in one region and concurrent examination of another region as task
427 performance improves. Implementing this strategy, we aimed to disentangle cerebello-
428 cortical communication as M1 direct control was learned. Importantly, both M1 and
429 cerebellum have direct connections to the spinal cord[8–10], and are implicated in movement
430 control[3,4,6]. In our BMI paradigm, we randomly selected target neural pattern in M1

431 (enforced by the decoder), which is unlikely to be correlated with processes in other brain
432 regions. This permitted us to examine how cross-area communication during BMI control
433 facilitates control. M1 and cerebellum are reciprocally connected[1,2], and while some
434 extent of coupling of task-related activity in M1 and cerebellum is not surprising, it is
435 unknown how the indirect cerebellum activity interacts with behavioral output specific
436 direct activity versus indirect or non-task specific activity of M1 neurons.
437
438 One of the striking findings of our work is that canonical correlation increased between
439 M1 TR_d and cerebellum TR_i units. Similarly, cross-correlograms between these unit pairs
440 also showed more coincident firing. However, this was not the case for M1 TR_i's and
441 cerebellum TR_i's. Cerebellum optogenetic inhibition also weakened modulation of M1 TR_d
442 's which suggests that the cerebellum communicated more strongly with task-specific
443 pools of M1 direct activity. These ideas are consistent with theoretical studies that
444 suggest that cerebellar cortex helps in task-relevant dimensionality expansion that aids
445 in learning[43].
446
447 ***Roles of multiplexed cross-area interactions***
448 Motor control involves signals at longer time scales appropriately integrating with shorter
449 time scales across several spatially segregated regions to deliver movement precision[44].
450 Little is known about how these signals at varying spatiotemporal scales are interacting
451 during motor control. Simultaneous recordings are best suited to understand these
452 interactions[6,36,36,45–47]. Further, a majority of studies that have used simultaneous
453 recordings in motor regions use extensively trained animals performing natural motor

454 tasks[46–49]. Understanding M1-cerebellum interactions in such context raises important
455 concerns: *(i)* since both M1 and cerebellum are directly controlling movement, it is difficult
456 to ascertain modulatory influence of one area over the other; and *(ii)* overtrained animals
457 may have transitioned to an 'automatic' state[50], and it may no longer be suitable to
458 investigate emergent dynamics in interacting structures. These confounds limit the
459 inferences about M1-cerebellum interactions in experiments with extensively trained
460 animals.
461
462 Here we have shown that in an M1-driven BMI task, cerebellum activity leads M1 direct
463 activity and hence, may play an instructional role in the beginning. This idea is consistent
464 with the notion of cerebellar role in skill acquisition[51]. We find that cerebellar indirect
465 activity leads later in learning as well, indicative of an ongoing modulatory influence over
466 M1 to sustain proficiency in the task. This is consistent with the notions of cerebellar
467 contributing to fine-tuning effector movements[42,52]. We also find that M1 indirect activity
468 is correlated to M1 direct activity, but not to cerebellar indirect activity. This leads us to
469 conclude that M1 output-specific neurons contain multiplexed signals coordinated with
470 both local and distant-area activity and that cerebellar activity might be somatotopically
471 organized; thus, the cerebellar activity is retained in the cortico-cerebellar loop[53]. Our
472 cross-correlation between M1 TR_d and cerebellum TR_i units also showed a broader
473 timescale influence of cerebellum on M1 activity (this is different from the shorter time
474 scale influences seen between M1 TR_d and M1 TR_i units[11]). Such broader influence of
475 cerebellar activity may be related to coordination in the larger motor network. Larger

476 network activity may represent attention regulation[54], motivation[55] or coordination of the
477 motor task with sensory feedback[56].
478
479 ***Neural dynamics over the course of BMI learning***
480 Natural motor learning is known to involve an early phase marked exploration and high
481 variability with a transition to late stage when the skill is consolidated[57–60]. Our paradigm
482 here is focused on early exploratory BMI learning by using mostly single-sessions. BMI
483 studies that allow for sleep consolidation[11,12,18] or use multiple days of learning[15,61] find
484 that M1 TR_i units weaken their modulation through the course of extensive training. It is
485 possible that cerebellar TR_i's may exhibit similar weakening over time. However, local
486 versus cross-area interactions may differ in the long-term. One recent study had focused
487 on cross-area activity through multiple days of training, and they found that indirect task-
488 related modulation persists in several cortical areas[23]. Work that has looked at extensively
489 trained mice on motor task has shown sustained activity in the cerebellum[42]. There is
490 further evidence from studies of natural learning that emergent activity in cortico-
491 cerebellar networks becomes stronger as task proficiency increases[7].
492
493 To summarize, our studies leveraged a multiarea BMI paradigm to probe M1-cerebellar
494 cross-area interactions. We demonstrated that oscillatory dynamics emerged as seen
495 through LFPs across these regions that also modulated task-related spiking in both areas.
496 Finer time scale analyses of spiking revealed that cerebellar indirect activity selectively
497 influenced our imposed artificial target activity pattern within M1. This paradigm allowed
498 us to manufacture an output-specific pattern, with a relatively small neural footprint to

examine internal motor networks dynamics, removing the constraints of movement performance. Thus, multiarea BMIs, through such impositions, allows for a more natural inside-out investigation of cross-area interactions.

502 **Methods**

503 **Animal preparation**

504 Adult male Long-Evans rats were used in this study (n = 13, 250–400 g, ~ 8 weeks old,
505 Charles River Laboratories). All animal procedures were performed according to the
506 protocol approved by the Institutional Animal Care and Use Committee at Cedars-Sinai
507 Medical Center, Los Angeles. This ensured that the animals that were used in this
508 research were acquired, cared for, housed, used, and disposed of in compliance with the
509 applicable federal, state, and local laws and regulations, institutional policies and with
510 international conventions to which the United States is a party. Animals were housed on
511 a 14 h light and 10 h dark cycle (Photoperiod is from 6 am to 8 pm) in a climate-controlled
512 vivarium. Out of 13 rats, 8 were used in BMI with simultaneous M1 and cerebellum
513 recordings, 3 rats were used for BMI with cerebellar optogenetic inhibition and the
514 remaining (n = 2) were used in acute cerebellar recording under optogenetic inhibition.
515 Neural probes were implanted during a recovery surgery performed under isofluorane (1–
516 3%) anesthesia. The analgesic regimen included the administration of 0.1 mg per kg body
517 weight buprenorphine, and 5 mg per kg body weight carprofen. Post-operatively, rats
518 were also administered 2 mg per kg body weight dexamethasone and 33 mg per kg body
519 weight sulfatrim for 5 days. Ground and reference screws were implanted posterior to
520 lambda contralateral to the recorded cerebellum, contralateral to the neural recordings.
521 For M1 recordings, 32-channel arrays (33-μm polyamide-coated tungsten microwire
522 arrays) were lowered to a depth of ~1,200–1,500 μm in either the left or right M1
523 depending on handedness. These were implanted centered at 0.5 mm anterior and 3 mm
524 lateral to the bregma (Ramanathan et al., 2015; Lemke et al., 2019). For cerebellar

525 recordings we used 32-64 channel tetrodes (Neuronexus, MI) or shuttle-mounted
526 polytrodes (Cambridge Neurophysiology, UK). The probes were lowered into the
527 cerebellar cortex through a craniotomy centered at 12.5 mm posterior and 2.5-3 mm
528 lateral to bregma. Shuttle mounted probes were moved across days and recorded from
529 depths of 1.5-4 mm. Our target regions were Simplex/ Crus I and Crus II areas of the
530 cerebellum (Atkins and Apps, 1997; Baker et al., 2001; Heck et al., 2007). Activity in these
531 areas has shown modulation during upper limb motor behaviors in response to
532 corticofugal fiber and forelimb stimulation. We did not perform subject-specific
533 implantation based on motor mapping. However, a subset of rats also performed reaching
534 tasks and had robust activation during reaching[7].
535
536 **Viral injections**
537 We used a red-shifted halorhodopsin, Jaws (AAV8-hSyn-Jaws-KGC-GFP-ER2, UNC
538 Viral Core) for neural silencing in 5 rats for optogenetic experiments[12,18,62]. Viral injections
539 were done at least 3 weeks before chronic implant surgeries. Rats were anesthetized, as
540 stated before and body temperature was maintained at 37 °C with a heating pad. Burr
541 hole craniotomies were performed over injection sites, and the virus was injected using a
542 Hamilton Syringe with 34G needle. 500-nl injections (100 nl per min) were made at two
543 sites in the cerebellum (11.5 mm posterior, 2.5 mm lateral to bregma and 11.5 mm
544 posterior and 3.5 mm lateral to bregma; depth of 1-3 mm). After the injections, the skin
545 was sutured, and the animals were allowed to recover with same regimen as stated
546 above. Viral expression was confirmed with fluorescence imaging.
547

548 **Electrophysiology**

549 Units and LFP activity were recorded using a 128-channel TDT-RZ2 system (Tucker-
550 Davis Technologies). Spike data were sampled at 24,414 Hz and LFP data at 1,017.3 Hz.
551 ZIF (zero insertion force) clip-based digital head stages from TDT were used that interface
552 the ZIF connector and the Intan RHD2000 chip that uses 192x gain. Only clearly
553 identifiable units with good waveforms and high signal-to-noise were used. The remaining
554 neural data was recorded for offline analysis. Behavior related timestamps (i.e. trial onset,
555 trial completion) were sent to the RZ2 analog input channel using an Arduino digital board
556 and synchronized to neural data.

557

558 We have used the term *'unit'* to refer to the sorted spike recordings from both the MEA
559 and silicon probe recordings. For both, we initially used an online sorting tool (Synapse,
560 TDT) for neuroprosthetic control. We used waveform shape and the presence of an
561 absolute/relative refractory period in the inter-spike interval (ISI) to judge quality of
562 isolation. Specifically, a voltage-based threshold was set based on visual inspection for
563 each channel that allowed for best separation between putative spikes and noise;
564 typically, this threshold was at least 4 standard deviations (SD) away from the mean.
565 Events were time-stamped and waveforms for each event were peak aligned. K-means
566 clustering was then performed across the entire data matrix of waveforms. Automated
567 sorting was performed by: (1) first over-clustering waveforms using a K-means algorithm
568 (i.e., split into many mini-clusters), (2) followed by a calculation of interface energy (a
569 nonlinear similarity metric that allows for an automated decision of whether mini-clusters

570 are actually part of the same cluster), and (3) followed by aggregation of similar clusters.
571 We conducted offline spike sorting in Plexon or Spyking Circus[63].
572
573 **Behavior**
574 After recovery, animals were typically acclimated for 1-2 day to a custom plexiglass
575 behavioral box (**Fig. 1a**) prior to the start of experimental sessions. After acclimatization,
576 rats were water restricted for BMI training. We monitored body weights daily to ensure
577 that the weight did not drop below 95% of the initial weight.
578
579 Behavioral sessions were typically conducted for 1-2 hours. Recorded neural data was
580 entered in real-time to custom routines in Matlab (R2018b; Mathworks, Natick, MA).
581 These then served as control signals for the angular velocity of the feeding tube. The rats
582 performed ~120 trials on an average in a session (e.g. **Fig. 1c**). In a subset of sessions
583 (n = 14), we also video-monitored the rat during the BMI training using a 30-fps camera
584 (TDT, USA).
585
586 **Neural control of the feeding tube**
587 During the BMI training sessions, we typically selected one or two M1 channels' units to
588 be selected as 'direct' (TR_d) units, and their neural activity was used to control the angular
589 velocity of the feeding tube. If one channel was choosen for neuroprosthetic control, its
590 neurons were associated with positive weight and if two channels were chosen, one
591 channels neurons were associated with a positive weight and another's with a negative
592 weight. These units maintained their stability throughout the recording as evidenced by

stability of waveform shape and interspike-interval histograms (**Supplementary Fig. 1**). We binned the spiking activity into 100ms bins. We then established a mean firing rate for each neuron over a 3–5 minute baseline period. The mean firing rate was then subtracted from its current firing rate at all time points. The specific transform that we used was:

$$\theta_v = C \times [G_1 \times r_1(i) + G_2 \times r_2(i)]$$

where θ_v was the angular velocity of the feeding tube, $r_1(i)$ and $r_2(i)$ were firing rates of the direct units. G_1 and G_2 were randomized coefficients that ranged from +1 to −1 and were held constant after initialization. C was a fixed constant that scaled the firing rates to angular velocity. The animals were then allowed to control the feeding tube via modulation of neural activity. The tube started at the same position at the start of each trial (P_1 in **Fig. 1a**). The calculated angular velocity was added to the previous angular position at each time step (100 ms). During each trial, the angular position could range from −45 to +180 degrees. If the tube stayed in the 'target zone' (P_2 in **Fig. 1a;** spanned 10° area) for a period of 400 ms, then a water reward was delivered. In the beginning of a session, most rats were unsuccessful at bringing the feeding tube to position P_2. Most rats steadily improved control and reduced the time to completion of the task during a session. Multiple learning sessions were obtained from each animal. Consistent with past studies, we also found that incorporation of new units into the control scheme required new learning[11,64–66].

616 **Optogenetics**

617 Optogenetic experiments was carried out in JAWS injected rats using a high-power laser
618 (50 W/mm^2: Laserglow Technologies, USA) emitting a 625 nm beam. A subset of rats (n
619 = 3) was implanted with a cannula over Crus I/Crus II region of the cerebellar cortex and
620 a 32-channel microwire array (TDT Florida) was implanted in M1. During the behavior
621 experiments, laser was turned on at every 10 ms at 50% duty cycle to inhibit cerebellar
622 activity after the trial onset for the total duration of the trial (15s). We performed two
623 sessions each day with ~100 trials in each session. Each day, we alternated between
624 turning the laser on in the first session or the second session (**Supplementary Fig. 6a**).
625 Another subset of rats (n = 2) was implanted with fiber-optic cannula mounted on a silicon
626 probe (Cambridge Neurotech, UK) in the cerebellum, and the recordings were performed
627 under isofluorane anesthesia. In every trial, we recorded 5s of baseline followed by 5s for
628 which the laser was on and another 5 s thereafter with laser off. We performed 30 such
629 repetitions.

630

631

632 **Histology**

633 After the experiment, rats were deeply anaesthetized with isoflurane (4-5%), then
634 exsanguinated and perfused with 4 % paraformaldehyde (PFA). The brains were
635 extracted and stored in 4% PFA for up to 72 hours. The brains were then transferred to a
636 solution of 30% sucrose and stored for sectioning. We performed sagittal or coronal
637 sections of the brain using a cryostat (Leica, Germany) and stored them in phosphate-
638 buffered saline for imaging. Images were mounted on slices and imaged using a

639 microscope (Keyence, Japan). The location and depth of the silicon probe in the brain
640 were traced by DiI depositing on the electrodes prior to their implantation and by looking
641 afterwards at the fluorescent dye present in the histological slices (**Supplementary Fig.**
642 **2**).
643
644
645 **Data Analysis**
646 *Sessions and changes in performance*
647 Analysis was performed in Matlab (R2020b) with custom-written routines. A total of 23
648 training sessions recorded from 8 rats were used for our initial analysis. In addition, we
649 analyzed 12 separate sessions across 3 rats where optogenetic inhibition of the
650 cerebellum was performed. For **Fig. 1b,c** we compared changes in task performance
651 across sessions. Specifically, we compared the performance change by calculating the
652 mean and standard error of the mean (s.e.m) of the time to completion during the first
653 and last 30% of trials (referred as early and late trials respectively). Furthermore, we also
654 compared the best performance in early and late trials by calculating the percentage of
655 unsuccessful trials.
656
657 *Task-related activity*
658 The distinction between TR_d, TR_i and *TU* units was based on whether significant
659 modulation of baseline firing activity after trial onset (i.e., peak of modulation at the time
660 > 2.5 SD above the baseline period).
661

662 *LFP analysis*

663 Artifact rejection was first performed on LFP signals to remove broken channels and noisy
664 trials. LFPs were then z-scored, median referenced and evoked-activity was subtracted
665 separately for M1 and cerebellum. LFP power was calculated on a trial-by-trial basis and
666 then averaged across channels and animals, with wavelet decomposition using the
667 EEGLAB function *newtimef*[67]. M1-Cb LFP coherence was calculated for each pair of
668 channels using the EEGLAB function *newcrossf*[67]. All the comparisons were done
669 between early and late trials. For this analysis, across all the early trials, only trials where
670 time to task completion was over 10 seconds were included. Across all the late trials, only
671 trials where time to task completion was under 5 seconds were included.

672

673 *Spike-triggered averaging (STA)*

674 We calculated the STA to measure how spikes locked to the 3-6 Hz LFP oscillations, both
675 in the M1 and the cerebellum. We used filtered (3–6Hz) median LFP from each region for
676 this analysis. For filtering, we used the EEGLAB function *eegfilt*. We used the first 4
677 seconds after the start of the trial to calculate these STAs. For every unit, we
678 concatenated the spikes from early trials in a spike vector and from late trials in another
679 vector. Before STA calculation, we equaled the length these vectors. Then, we extracted
680 2 sec of LFP around every spike-time in those vectors and average it to get early and late
681 STAs for a given unit. To calculate the change in modulation for every unit, we looked at
682 the difference between the minimum and maximum peak in a 300 ms window around a
683 spike in the averaged STA of early and late trails and then calculated this change from
684 early to late trials in percentage. We also calculated STA during inter-trial interval. Here,

685 we used from 2 to 6 seconds after the end of the trial and applied the same steps to
686 compute the STA as described above.
687
688 *Spike cross-correlation*
689 We computed the cross-correlation histogram (CCH) for M1 TR_d – cerebellar TR_i, M1 TR_i
690 – cerebellar TR_i and M1 TR_d -M1 TR_i unit pairs. For every trial, the spike counts were
691 equalized between the pairs before computing the CCH using 10 ms bins. Furthermore,
692 we constructed pseudo-random spike train CCHs with simulated spike counts of equal
693 length for every pairing. Such simulations were run 300 times (Monte Carlo
694 Simulations)[11,68]. To quantify pairwise coincident firing from early to late trials, we took
695 the mean of the simulated CCH magnitude within ± 400 ms around the center and
696 subtracted it from the mean of real CCH magnitude in the same window for early and late
697 trials, respectively (*ΔCCH*).
698
699 *Canonical correlation analysis*
700 CCA identifies maximally correlated linear combinations between two groups of variables.
701 Unit spiking data in M1 and cerebellum from -2 s to + 2 s around task-start for each trial
702 were binned at 100ms and concatenated. CCA models were then fit using the MATLAB
703 function *canoncorr*. Only the top canonical component was used in this paper.
704
705 *Video tracking & trajectory analysis*
706 We performed automated tracking of the tip of the feeding tube and the implanted forepaw
707 of the rats using DeepLabCut[69]. We did cross-correlation between the trajectories of the

708 feeding tube and the forepaw using *xcorr* function of MATLAB and looked at the average
709 cross-correlation magnitude ±30ms around zero lag for every trial.
710
711 *Statistical analysis*
712 All statistical analyses were implemented within MATLAB. The linear mixed-effects model
713 (implemented using MATLAB *fitlme*) was used to compare the differences in behavior,
714 trial to mean correlation, speed decoding and canonical correlation unless specified
715 otherwise. This model accounts for the fact that units or sessions from the same animal
716 are more correlated than those from different animals and is more stringent than
717 computing statistical significance over all units and sessions[6,40,70]. We fitted random
718 intercepts for each rat and reported the *p*-values for the regression coefficients associated
719 with sessions, channels, or units. We also performed Kruskal-Wallis H-test with multiple
720 comparisons in **Fig. 3c** and **d**.
721

722 **Supplementary Figures**

723

724

725

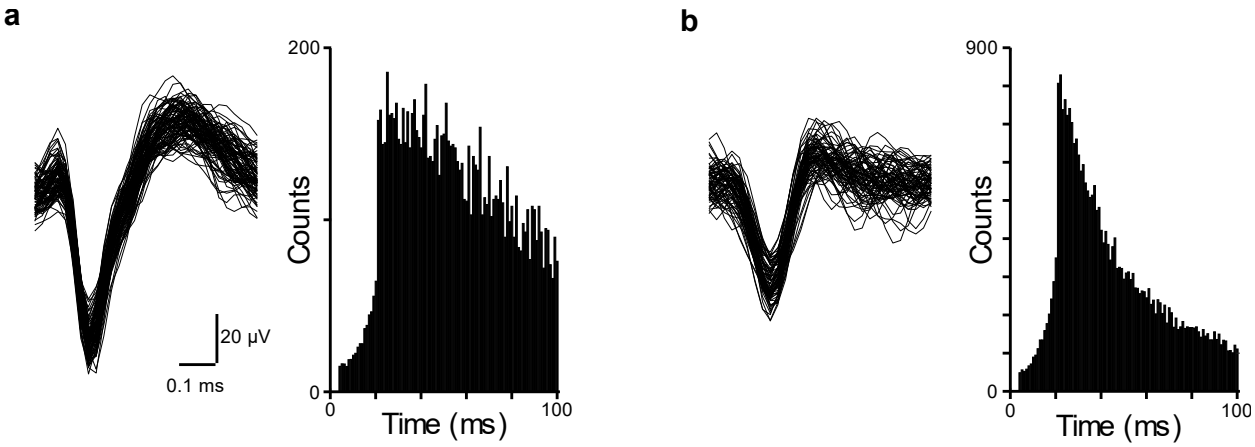

726

727 **Supplementary Figure 1. Single Unit Waveforms and Inter-Spike Interval (ISI).** ***a*****,** Left
728 panel shows waveforms of a representative M1 TR_d unit. Right panel shows ISI
729 histograms for the same unit. ***b*****,** Left panel shows waveforms of a representative task-
730 related M1 TR_i unit. Right panel shows ISI histograms for the corresponding units in the
731 left panel.
732

733

734

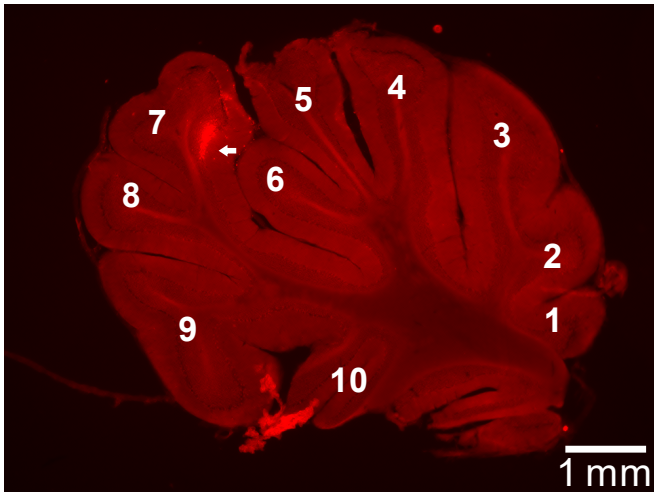

Supplementary Figure 2. Cerebellum electrode localization. The location of the electrode in lobule 7 of the cerebellum is indicated by a white arrow in the image of a brain section 4.75 mm lateral to the midline.

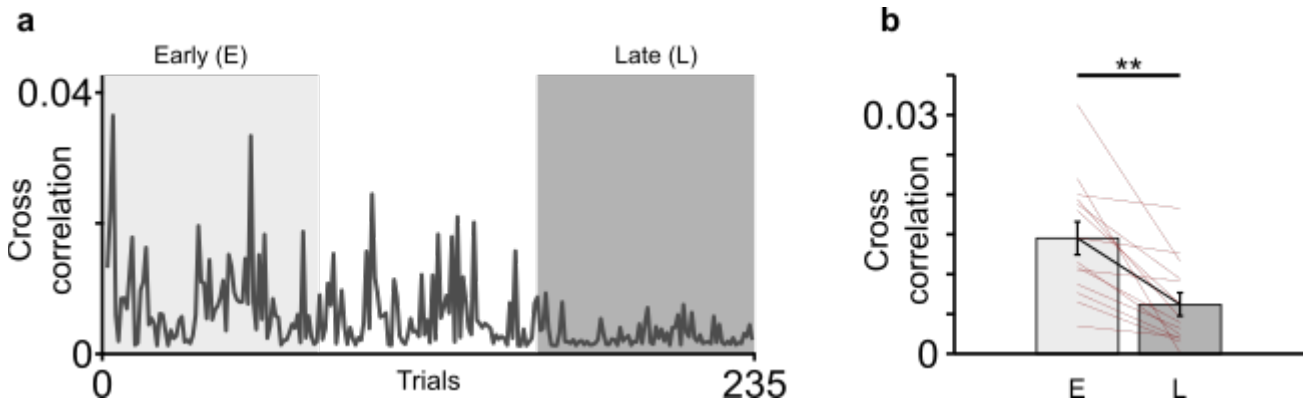

Supplementary Figure 3. Movement correlation reduces between forepaw and feeding tube *a*, Decrease in movement correlation in an example session ***b*,** Correlation reduces from early to late trials. **p<0.01.

754

755

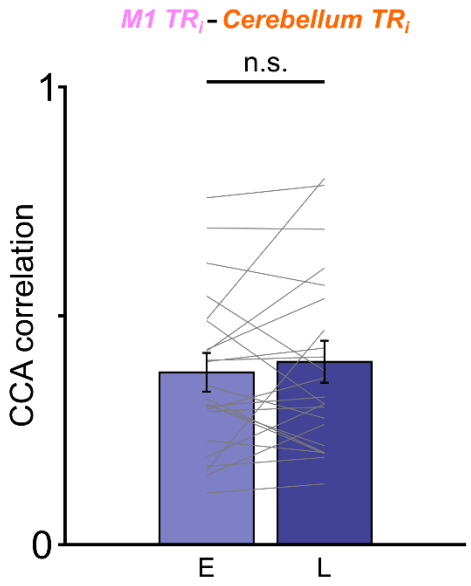

756

757 **Supplementary Figure 4. Canonical correlation analysis for M1 and cerebellum**
758 **units.** Change in CCA correlation shown between M1 and cerebellum task-related
759 indirect (*TR*$_i$) units. (n.s.; p>0.5)**.**
760

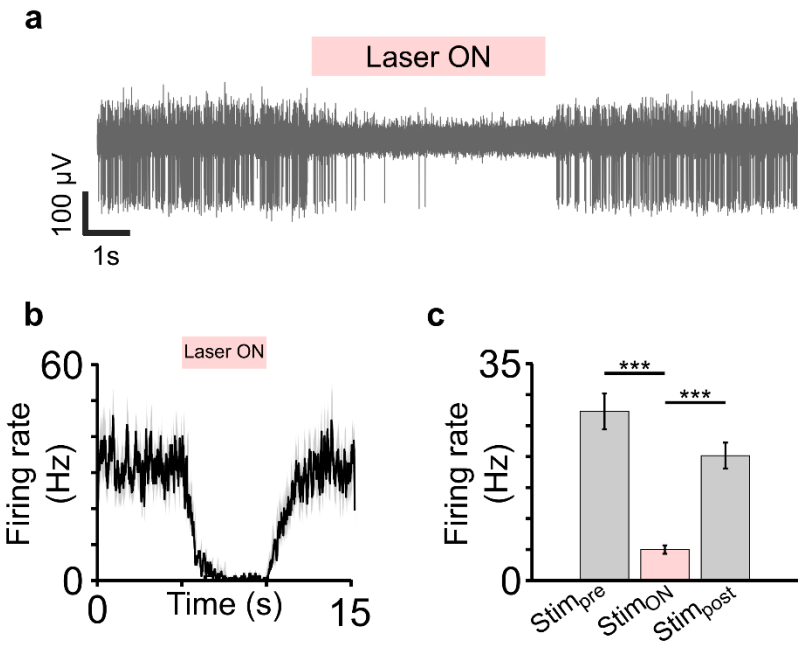

Supplementary Figure 5. Inhibition of cerebellar neural activity with optogenetic illumination *a*, A raw trace from an example channel showing reduction in acttvity when the laser was turned on. ***b*,** PSTH of an example unit showing reduction in firnig rate with laser on. ***c*,** Change in the firing rate of all the recorded units before, during and after cerebellar inhibition. ***p<0.001.

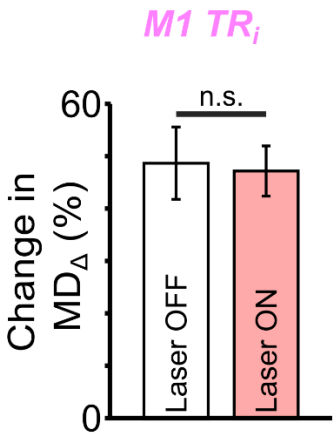

Supplementary Figure 6. Effect of cerebellar inhibition on *'indirect'* M1 units Change in modulation depth (MD_{Δ}) of M1 TR_i units from *early* to *late* trials, with and without cerebellar inhibition. $^{n.s.}p>0.05$.

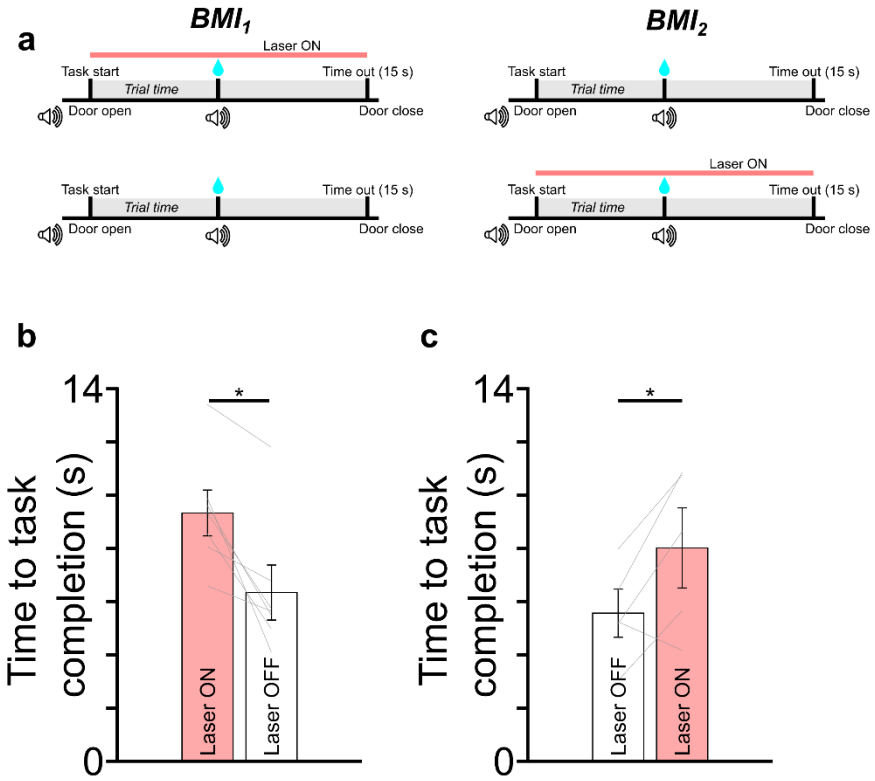

Supplementary Figure 7. Cerebellar inhibition impairs BMI performace during task acquisition and maintanence. *a*, Schematic of session structure. On a day, initial session were performed with cerebellar inhibition trials (Laser ON) followed by subsequent session without cerebellar inhibition (top). Next day, the order was inverted with initial sessions' trials without cerebellar inhibition performed first followed by subsequent trials with cerebellar inhibition (bottom). ***b*** and ***c*,** An increase in the time to task completion was observed irrespective of the order of cerebellar stimulation.

Acknowledgements

We thank Celine Riera and Joshua Burda for resources and reagents for histology, and Pierson Fleischer for insightful feedback during discussion. This research is supported by American Heart Association (postdoctoral fellowship 897265 to A.A. and career development award 847486 to T.G.), National Institutes of Health (R00NS097620 to T.G.), National Science Foundation (CAREER award 2048231 to T.G.) and Cedars-Sinai Medical Center. A.A. also received support from a Cedars-Sinai's Center for Neural Science and Medicine postdoctoral fellowship.

Author Contributions

A.A. and T.G. designed the study. A.A., A.W.F. and N.P.D. carried out the electrophysiology experiments. A.A., A.W.F., N.P.D. and T.G. performed the surgical procedures. A.A. carried out the analysis. A.W.F. and N.P.D. assisted with analysis. A.W.F. and N.P.D. carried out histology. A.A. and T.G. wrote the manuscript. A.W.F. edited the manuscript.

References

1. Kelly, R. M. & Strick, P. L. Cerebellar Loops with Motor Cortex and Prefrontal Cortex of a Nonhuman Primate. *J. Neurosci.* **23**, 8432–8444 (2003).
2. Wagner, M. J. *et al.* Shared Cortex-Cerebellum Dynamics in the Execution and Learning of a Motor Task. *Cell* vol. 177 669-682 e24 (2019).
3. Bloedel, J. R., Bracha, V., Milak, M. & Shimansky, Y. Cerebellar contributions to the acquisition and execution of learned reflex and volitional movements. *Prog Brain Res* vol. 114 499–509 (1997).
4. Heck, D., Kummell, F., Thach W. T. & Aertsena, A. Dynamic Correlation of Neuronal Activity in Rat Cerebellar Cortex Modulated by Behavior. *Annals of the New York Academy of Sciences* vol. 978 156–163 (2002).
5. Ramanathan, D. S., Gulati, T. & Ganguly, K. Sleep-Dependent Reactivation of Ensembles in Motor Cortex Promotes Skill Consolidation. *PLoS Biol* vol. 13 e1002263 (2015).
6. Lemke, S. M., Ramanathan, D. S., Guo, L., Won, S. J. & Ganguly, K. Emergent modular neural control drives coordinated motor actions. *Nat Neurosci* vol. 22 1122–1131 (2019).
7. Fleischer, P. J. *et al.* Emergent low-frequency activity in cortico-cerebellar networks with motor skill learning. 2022.05.18.491978 (2022) doi:10.1101/2022.05.18.491978.
8. Dum, R. P. & Strick, P. L. Motor areas in the frontal lobe of the primate. *Physiol. Behav.* **77**, 677–682 (2002).
9. Nudo, R. J. & Masterton, R. B. Descending pathways to the spinal cord, III: Sites of origin of the corticospinal tract. *J. Comp. Neurol.* **296**, 559–583 (1990).
10. Pompeiano, O. Functional Organization of the Cerebellar Projections to the Spinal Cord. in *Progress in Brain Research* (eds. Fox, C. A. & Snider, R. S.) vol. 25 282–321 (Elsevier, 1967).
11. Gulati, T., Ramanathan, D. S., Wong, C. C. & Ganguly, K. Reactivation of emergent task-related ensembles during slow-wave sleep after neuroprosthetic learning. *Nat Neurosci* vol. 17 1107–13 (2014).
12. Gulati, T., Guo, L., Ramanathan, D. S., Bodepudi, A. & Ganguly, K. Neural reactivations during sleep determine network credit assignment. *Nature Neuroscience* vol. 20 1277–1284 (2017).
13. Arduin, P. J., Fregnac, Y., Shulz, D. E. & Ego-Stengel, V. 'Master' neurons induced by operant conditioning in rat motor cortex during a brain-machine interface task. *J Neurosci* vol. 33 8308–8320 (2013).
14. Sadtler, P. T. *et al.* Neural constraints on learning. *Nature* vol. 512 423–6 (2014).
15. Ganguly, K., Dimitrov, D. F., Wallis, J. D. & Carmena, J. M. Reversible large-scale modification of cortical networks during neuroprosthetic control. *Nat Neurosci* vol. 14 662–667 (2011).
16. Taylor, D. M., Tillery, S. I. & Schwartz, A. B. Direct cortical control of 3D neuroprosthetic devices. *Science* vol. 296 1829–1832 (2002).
17. Athalye, V. R., Ganguly, K., Costa, R. M. & Carmena, J. M. Emergence of Coordinated Neural Dynamics Underlies Neuroprosthetic Learning and Skillful Control. *Neuron* **93**, 955-970.e5 (2017).

18. Kim, J., Gulati, T. & Ganguly, K. Competing Roles of Slow Oscillations and Delta Waves in Memory Consolidation versus Forgetting. *Cell* vol. 179 514-526 e13 (2019).
19. Fetz, E. E. Volitional control of neural activity: implications for brain-computer interfaces. *J Physiol* vol. 579 571–579 (2007).
20. Koralek, A. C., Costa, R. M. & Carmena, J. M. Temporally precise cell-specific coherence develops in corticostriatal networks during learning. *Neuron* vol. 79 865–872 (2013).
21. Koralek, A. C., Jin, X., Long 2nd, J. D., Costa, R. M. & Carmena, J. M. Corticostriatal plasticity is necessary for learning intentional neuroprosthetic skills. *Nature* vol. 483 331–335 (2012).
22. Clancy, K. B., Koralek, A. C., Costa, R. M., Feldman, D. E. & Carmena, J. M. Volitional modulation of optically recorded calcium signals during neuroprosthetic learning. *Nature Neuroscience* (2014) doi:10.1038/nn.3712.
23. Liu, Z. & Schieber, M. H. Neuronal Activity Distributed in Multiple Cortical Areas during Voluntary Control of the Native Arm or a Brain-Computer Interface. *eNeuro* **7**, (2020).
24. Canolty, R. T. *et al.* Oscillatory phase coupling coordinates anatomically dispersed functional cell assemblies. *Proc Natl Acad Sci U S A* vol. 107 17356–17361 (2010).
25. Buzsaki, G. & Draguhn, A. Neuronal oscillations in cortical networks. *Science* vol. 304 1926–1929 (2004).
26. Fröhlich, F. & McCormick, D. A. Endogenous Electric Fields May Guide Neocortical Network Activity. *Neuron* **67**, 129–143 (2010).
27. Tiesinga, P. H. E., Fellous, J.-M., José, J. V. & Sejnowski, T. J. Optimal information transfer in synchronized neocortical neurons. *Neurocomputing* **38–40**, 397–402 (2001).
28. Harris, K. D., Csicsvari, J., Hirase, H., Dragoi, G. & Buzsáki, G. Organization of cell assemblies in the hippocampus. *Nature* **424**, 552–556 (2003).
29. Rodriguez, E. *et al.* Perception's shadow: long-distance synchronization of human brain activity. *Nature* **397**, 430–433 (1999).
30. Pesaran, B., Nelson, M. J. & Andersen, R. A. Free choice activates a decision circuit between frontal and parietal cortex. *Nature* **453**, 406–409 (2008).
31. Pesaran, B., Pezaris, J. S., Sahani, M., Mitra, P. P. & Andersen, R. A. Temporal structure in neuronal activity during working memory in macaque parietal cortex. *Nat. Neurosci.* **5**, 805–811 (2002).
32. Meer, M. A. A. van der & Redish, A. D. Theta Phase Precession in Rat Ventral Striatum Links Place and Reward Information. *J. Neurosci.* **31**, 2843–2854 (2011).
33. Fries, P., Womelsdorf, T., Oostenveld, R. & Desimone, R. The Effects of Visual Stimulation and Selective Visual Attention on Rhythmic Neuronal Synchronization in Macaque Area V4. *J. Neurosci.* **28**, 4823–4835 (2008).
34. Minxha, J., Adolphs, R., Fusi, S., Mamelak, A. N. & Rutishauser, U. Flexible recruitment of memory-based choice representations by the human medial frontal cortex. *Science* **368**, eaba3313 (2020).
35. DeCoteau, W. E. *et al.* Learning-related coordination of striatal and hippocampal theta rhythms during acquisition of a procedural maze task. *Proc. Natl. Acad. Sci.* **104**, 5644–5649 (2007).

36. Semedo, J. D., Zandvakili, A., Machens, C. K., Yu, B. M. & Kohn, A. Cortical Areas Interact through a Communication Subspace. *Neuron* **102**, 249-259.e4 (2019).
37. Veuthey, T. L., Derosier, K., Kondapavulur, S. & Ganguly, K. Single-trial cross-area neural population dynamics during long-term skill learning. *Nat. Commun.* **11**, 4057 (2020).
38. Gallego, J. A. *et al.* Cortical population activity within a preserved neural manifold underlies multiple motor behaviors. *Nat. Commun.* **9**, 4233 (2018).
39. Sussillo, D., Churchland, M. M., Kaufman, M. T. & Shenoy, K. V. A neural network that finds a naturalistic solution for the production of muscle activity. *Nat. Neurosci.* **18**, 1025–1033 (2015).
40. Guo, L., Kondapavulur, S., Lemke, S. M., Won, S. J. & Ganguly, K. Coordinated increase of reliable cortical and striatal ensemble activations during recovery after stroke. *Cell Rep.* **36**, 109370 (2021).
41. Sauerbrei, B. A. *et al.* Cortical pattern generation during dexterous movement is input-driven. *Nature* **577**, 386–391 (2020).
42. Becker, M. I. & Person, A. L. Cerebellar Control of Reach Kinematics for Endpoint Precision. *Neuron* vol. 103 335-348 e5 (2019).
43. Litwin-Kumar, A., Harris, K. D., Axel, R., Sompolinsky, H. & Abbott, L. F. Optimal Degrees of Synaptic Connectivity. *Neuron* **93**, 1153-1164.e7 (2017).
44. Doya, K. Complementary roles of basal ganglia and cerebellum in learning and motor control. *Curr. Opin. Neurobiol.* **10**, 732–739 (2000).
45. Perich, M. G. & Rajan, K. Rethinking brain-wide interactions through multi-region 'network of networks' models. *Curr. Opin. Neurobiol.* **65**, 146–151 (2020).
46. Perich, M. G., Gallego, J. A. & Miller, L. E. A Neural Population Mechanism for Rapid Learning. *Neuron* **100**, 964-976.e7 (2018).
47. Stringer, C. *et al.* Spontaneous behaviors drive multidimensional, brainwide activity. *Science* **364**, eaav7893 (2019).
48. Kaufman, M. T., Churchland, M. M., Ryu, S. I. & Shenoy, K. V. Cortical activity in the null space: permitting preparation without movement. *Nat. Neurosci.* **17**, 440–448 (2014).
49. Musall, S., Kaufman, M. T., Juavinett, A. L., Gluf, S. & Churchland, A. K. Single-trial neural dynamics are dominated by richly varied movements. *Nat. Neurosci.* **22**, 1677–1686 (2019).
50. Kawai, R. *et al.* Motor Cortex Is Required for Learning but Not for Executing a Motor Skill. *Neuron* **86**, 800–812 (2015).
51. Cantarero, G. *et al.* Cerebellar Direct Current Stimulation Enhances On-Line Motor Skill Acquisition through an Effect on Accuracy. *J. Neurosci.* **35**, 3285–3290 (2015).
52. Guo, J.-Z. *et al.* Disrupting cortico-cerebellar communication impairs dexterity. *eLife* **10**, e65906 (2021).
53. van der Zwaag, W. *et al.* Digit somatotopy in the human cerebellum: A 7T fMRI study. *NeuroImage* **67**, 354–362 (2013).
54. Ravizza, S. M. & Ivry, R. B. Comparison of the Basal Ganglia and Cerebellum in Shifting Attention. *J. Cogn. Neurosci.* **13**, 285–297 (2001).
55. Wagner, M. J. & Luo, L. Neocortex–Cerebellum Circuits for Cognitive Processing. *Trends Neurosci.* **43**, 42–54 (2020).

56. Wolpert, D., Ghahramani, Z. & Jordan, M. An internal model for sensorimotor integration. *Science* vol. 269 1880–1882 (1995).
57. Hikosaka, O., Nakamura, K., Sakai, K. & Nakahara, H. Central mechanisms of motor skill learning. *Curr. Opin. Neurobiol.* **12**, 217–222 (2002).
58. Kleim, J. A. *et al.* Cortical Synaptogenesis and Motor Map Reorganization Occur during Late, But Not Early, Phase of Motor Skill Learning. *J. Neurosci.* **24**, 628–633 (2004).
59. Floyer-Lea, A. & Matthews, P. M. Distinguishable Brain Activation Networks for Short- and Long-Term Motor Skill Learning. *J. Neurophysiol.* **94**, 512–518 (2005).
60. Luft, A. R. & Buitrago, M. M. Stages of motor skill learning. *Mol. Neurobiol.* **32**, 205–216 (2005).
61. Silversmith, D. B. *et al.* Plug-and-play control of a brain-computer interface through neural map stabilization. *Nat Biotechnol* (2020) doi:10.1038/s41587-020-0662-5.
62. Chuong, A. S. *et al.* Noninvasive optical inhibition with a red-shifted microbial rhodopsin. *Nature Neuroscience* vol. 17 1123–1129 (2014).
63. Yger, P. *et al.* A spike sorting toolbox for up to thousands of electrodes validated with ground truth recordings in vitro and in vivo. *eLife* **7**, e34518 (2018).
64. Moritz, C. T., Perlmutter, S. I. & Fetz, E. E. Direct control of paralysed muscles by cortical neurons. *Nature* vol. 456 639–642 (2008).
65. Gilja, V. *et al.* A high-performance neural prosthesis enabled by control algorithm design. *Nat Neurosci* vol. 15 1752–1757 (2012).
66. Ganguly, K. & Carmena, J. M. Emergence of a stable cortical map for neuroprosthetic control. *PLoS Biol* vol. 7 e1000153 (2009).
67. Delorme, A. & Makeig, S. EEGLAB: an open source toolbox for analysis of single-trial EEG dynamics including independent component analysis. *J. Neurosci. Methods* **134**, 9–21 (2004).
68. Abbasi, A. *et al.* Epidural cerebellar stimulation drives widespread neural synchrony in the intact and stroke perilesional cortex. *J. NeuroEngineering Rehabil.* **18**, 89 (2021).
69. Mathis, A. *et al.* DeepLabCut: markerless pose estimation of user-defined body parts with deep learning. *Nat Neurosci* vol. 21 1281–1289 (2018).
70. Aarts, E., Verhage, M., Veenvliet, J. V., Dolan, C. V. & van der Sluis, S. A solution to dependency: using multilevel analysis to accommodate nested data. *Nat Neurosci* vol. 17 491–6 (2014).

Figure 1

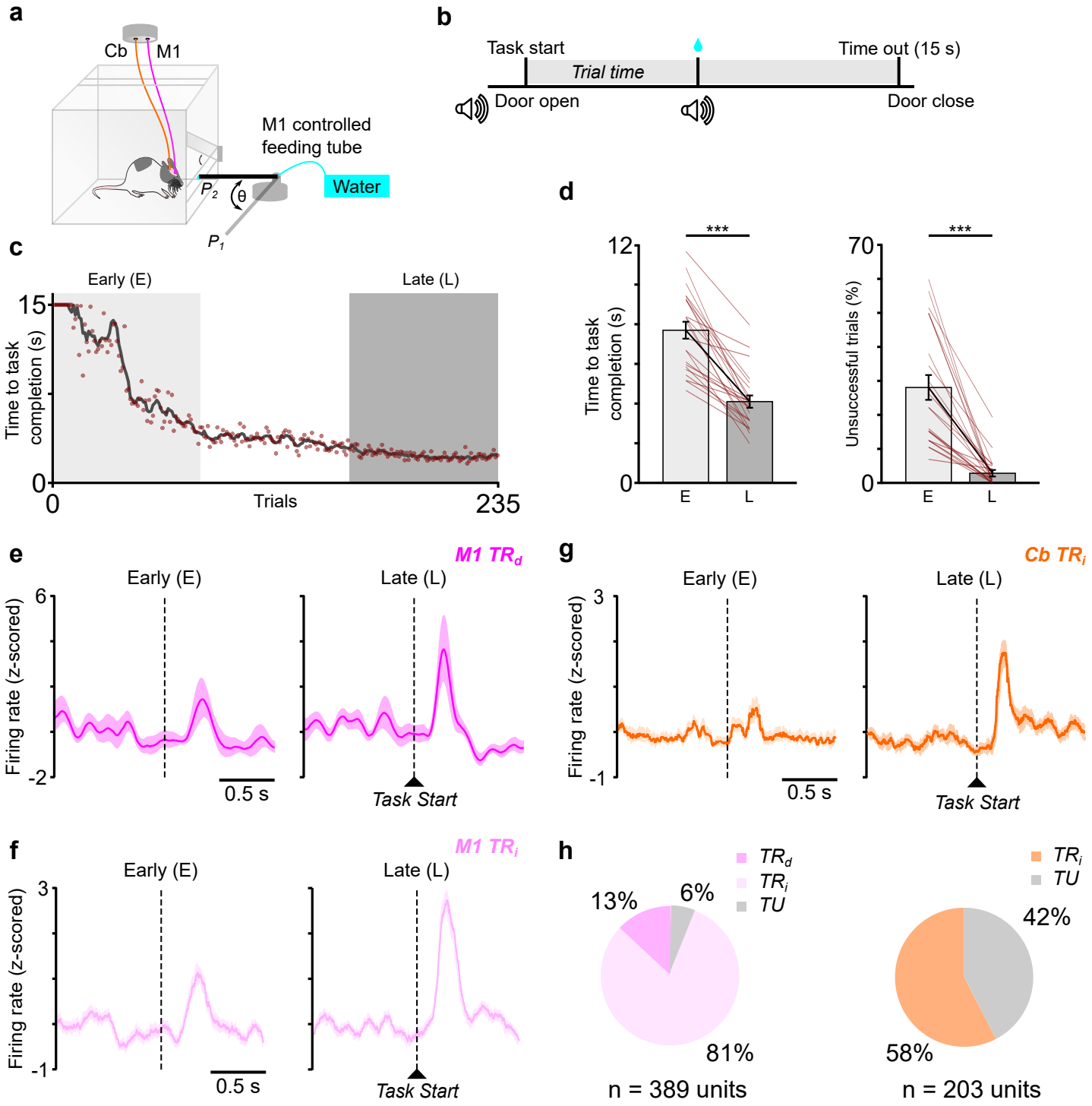
a
Cb
M1
M1 controlled
feeding tube
Water
P_2
θ
P_1
b
Task start
Trial time
Time out (15 s)
Door open
Door close
c
Early (E)
Late (L)
15
0
Time to task
completion (s)
0
Trials
235
d
***
12
0
Time to task
completion (s)
E
L
***
70
0
Unsuccessful trials (%)
E
L
e
M1 TR_d
Early (E)
Late (L)
6
-2
Firing rate (z-scored)
0.5 s
Task Start
g
Cb TR_i
Early (E)
Late (L)
3
-1
Firing rate (z-scored)
0.5 s
Task Start
f
M1 TR_i
Early (E)
Late (L)
3
-1
Firing rate (z-scored)
0.5 s
Task Start
h
TR_d
TR_i
TU
13%
6%
81%
n = 389 units
TR_i
TU
42%
58%
n = 203 units

Figure 2

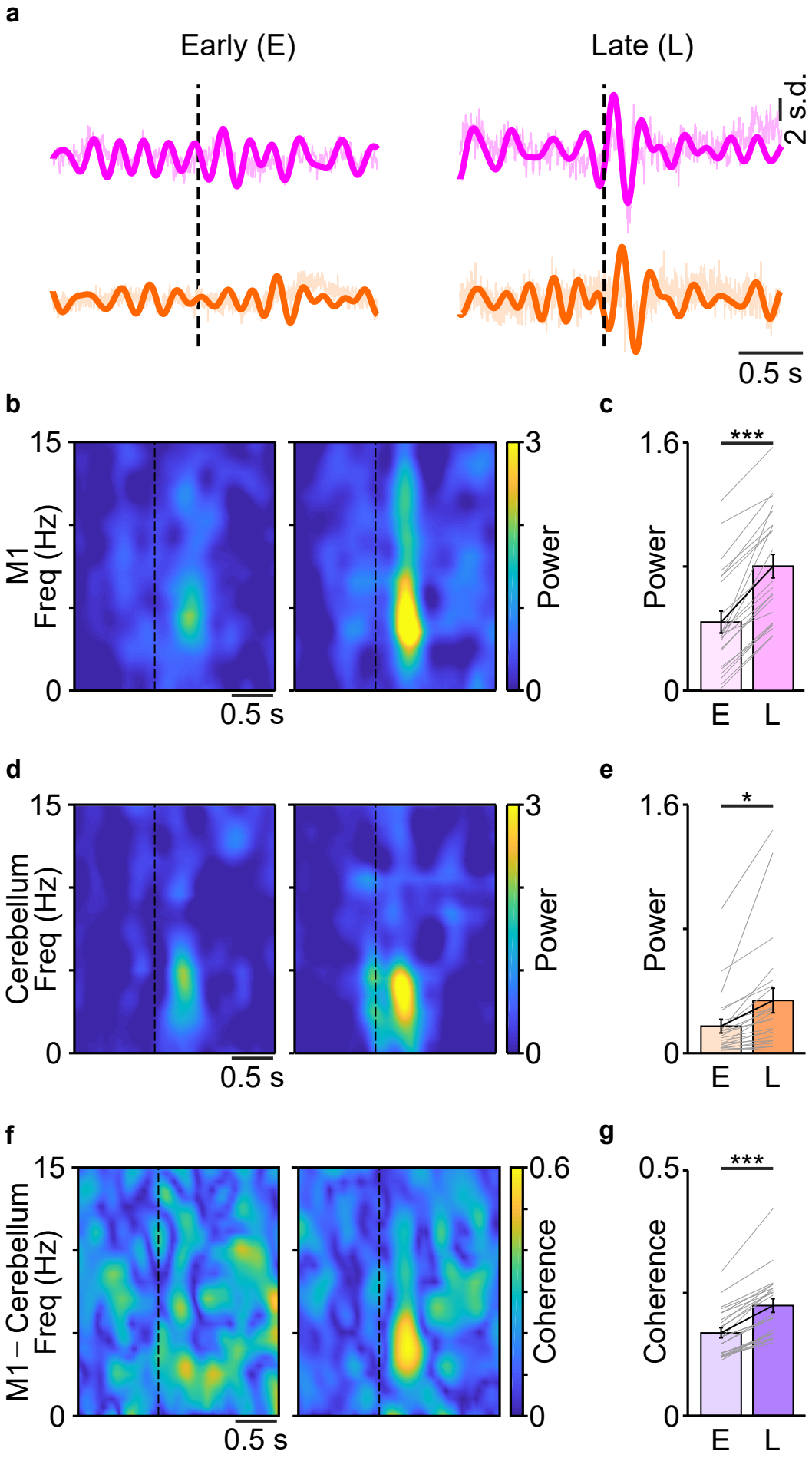
a
Early (E)
Late (L)
2 s.d.
0.5 s
b
c
15
M1
Freq (Hz)
0
0.5 s
3
Power
0
1.6
***
Power
0
E
L
d
e
15
Cerebellum
Freq (Hz)
0
0.5 s
3
Power
0
1.6
*
Power
0
E
L
f
g
15
M1 – Cerebellum
Freq (Hz)
0
0.5 s
0.6
Coherence
0
0.5
***
Coherence
0
E
L

Figure 3

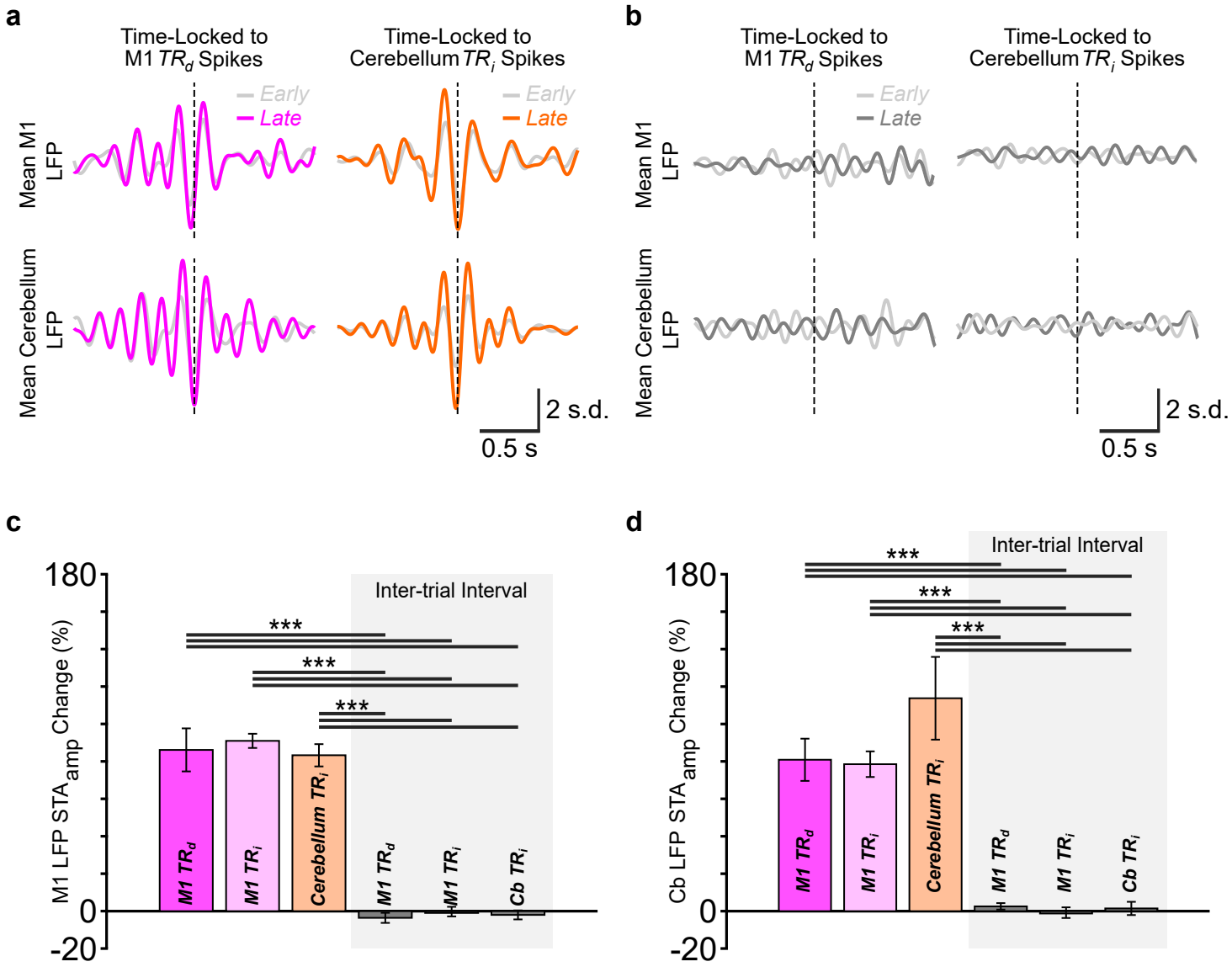
a
Time-Locked to M1 TR_d Spikes
Time-Locked to Cerebellum TR_i Spikes
Early
Late
Mean M1 LFP
Mean Cerebellum LFP
2 s.d.
0.5 s
b
Time-Locked to M1 TR_d Spikes
Time-Locked to Cerebellum TR_i Spikes
Early
Late
Mean M1 LFP
Mean Cerebellum LFP
2 s.d.
0.5 s
c
M1 LFP STA_{amp} Change (%)
180
0
-20
Inter-trial Interval
***
***
***
M1 TR_d
M1 TR_i
Cerebellum TR_i
M1 TR_d
M1 TR_i
Cb TR_i
d
Cb LFP STA_{amp} Change (%)
180
0
-20
Inter-trial Interval
***
***
***
M1 TR_d
M1 TR_i
Cerebellum TR_i
M1 TR_d
M1 TR_i
Cb TR_i

Figure 4

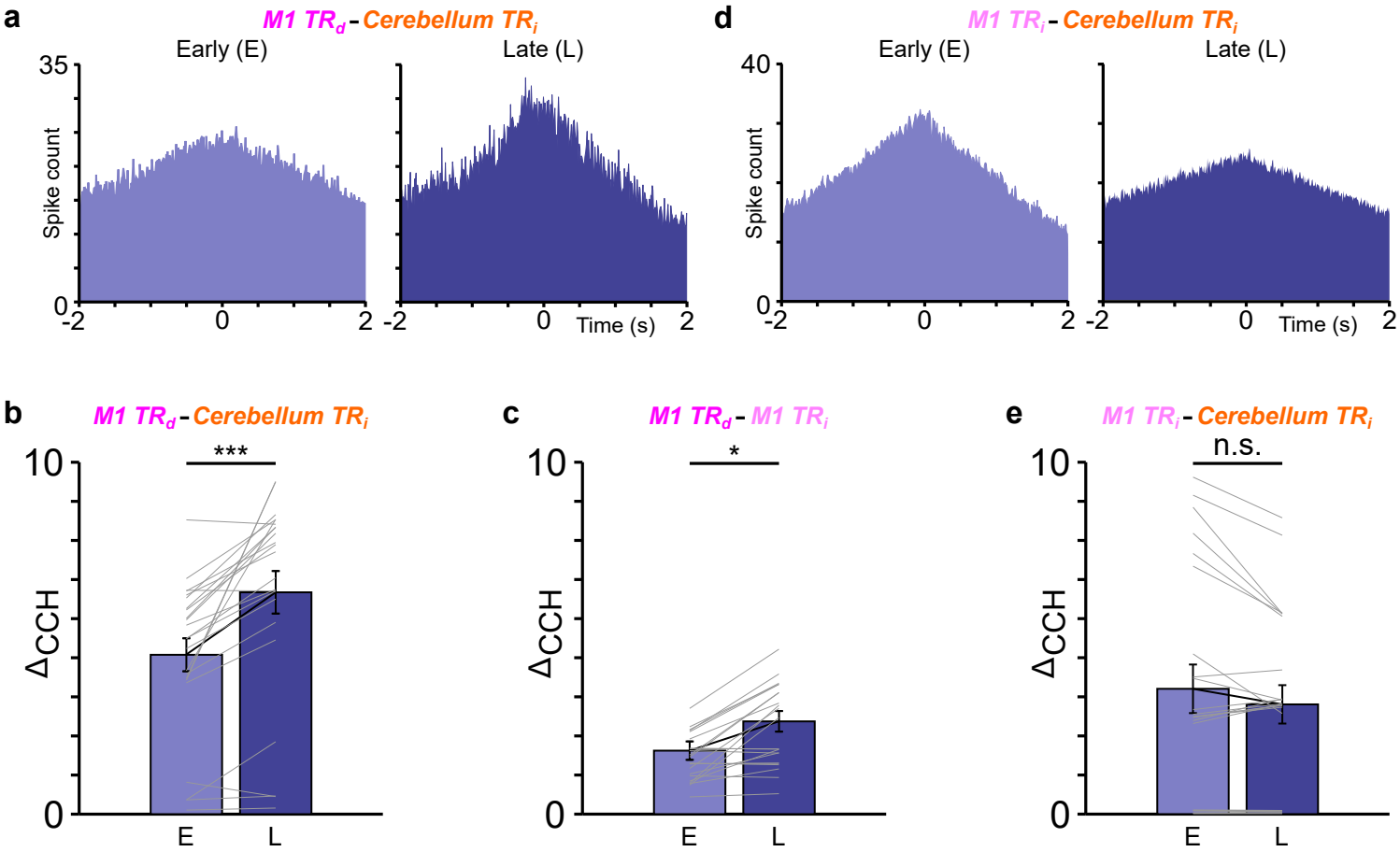
a
M1 TRd - Cerebellum TRi
Early (E)
Late (L)
35
0
Spike count
-2
0
2
Time (s)
d
M1 TRi - Cerebellum TRi
40
b
c
e
10
ΔCCH
***
*
n.s.
E
L

Figure 5

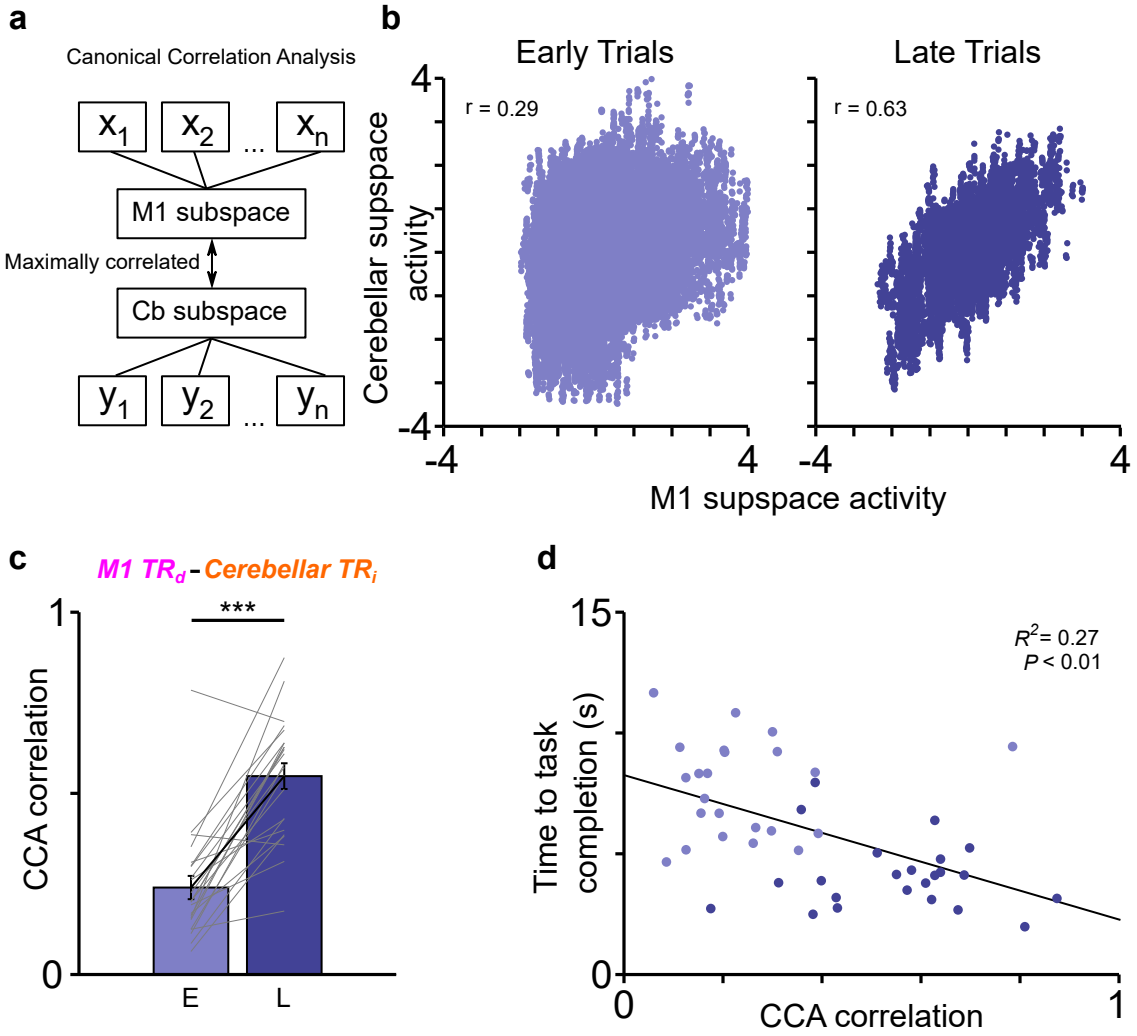
a
Canonical Correlation Analysis
x1
x2
...
xn
M1 subspace
Maximally correlated
Cb subspace
y1
y2
...
yn
b
Early Trials
Late Trials
r = 0.29
r = 0.63
Cerebellar supspace activity
M1 supspace activity
4
-4
-4
4
-4
4
c
M1 TRd - Cerebellar TRi
***
CCA correlation
1
0
E
L
d
R2 = 0.27
P < 0.01
Time to task completion (s)
CCA correlation
15
0
0
1

Figure 6

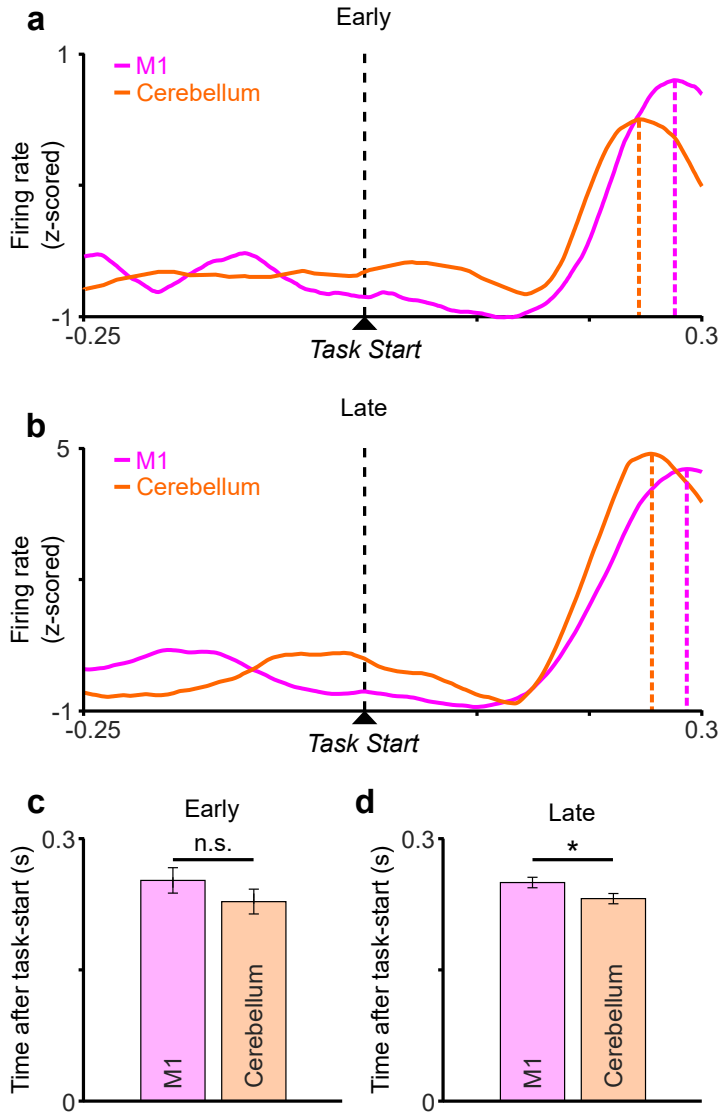
a
Early
M1
Cerebellum
Firing rate
(z-scored)
1
-1
-0.25
Task Start
0.3
b
Late
M1
Cerebellum
Firing rate
(z-scored)
5
-1
-0.25
Task Start
0.3
c
Early
n.s.
Time after task-start (s)
0.3
0
M1
Cerebellum
d
Late
*
Time after task-start (s)
0.3
0
M1
Cerebellum

Figure 7

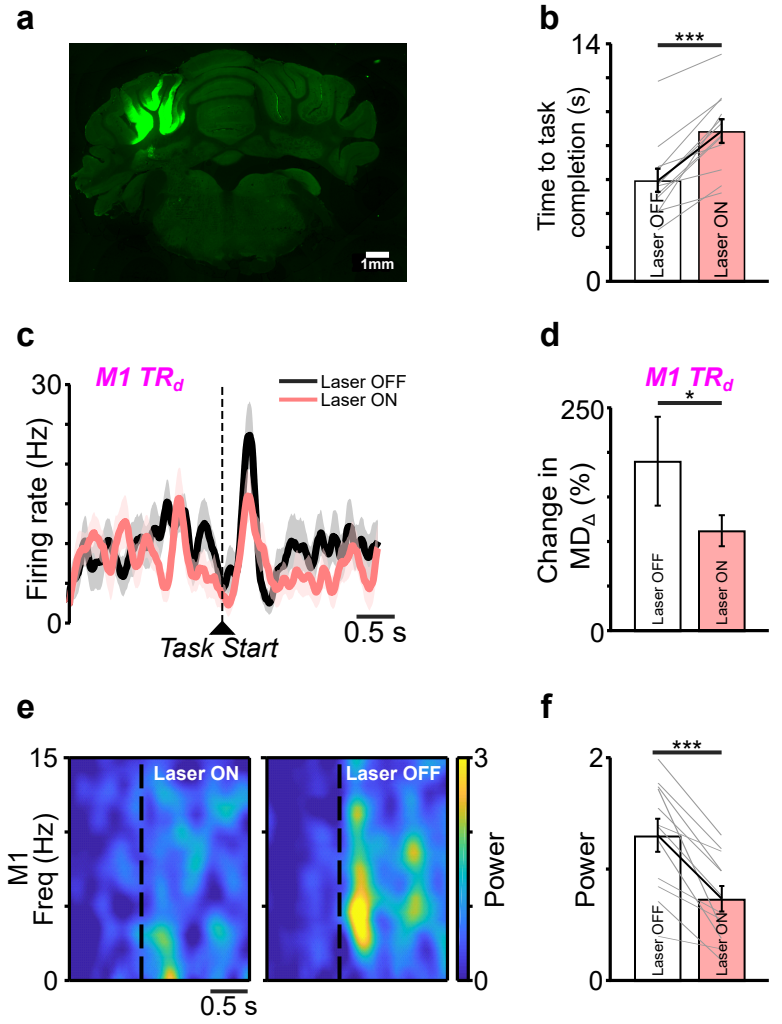
a
1mm
b
14
0
***
Time to task completion (s)
Laser OFF
Laser ON
c
M1 TRd
30
0
Firing rate (Hz)
Laser OFF
Laser ON
Task Start
0.5 s
d
M1 TRd
250
0
*
Change in MDΔ (%)
Laser OFF
Laser ON
e
15
0
M1 Freq (Hz)
Laser ON
Laser OFF
3
0
Power
0.5 s
f
2
0
***
Power
Laser OFF
Laser ON

Figure S1

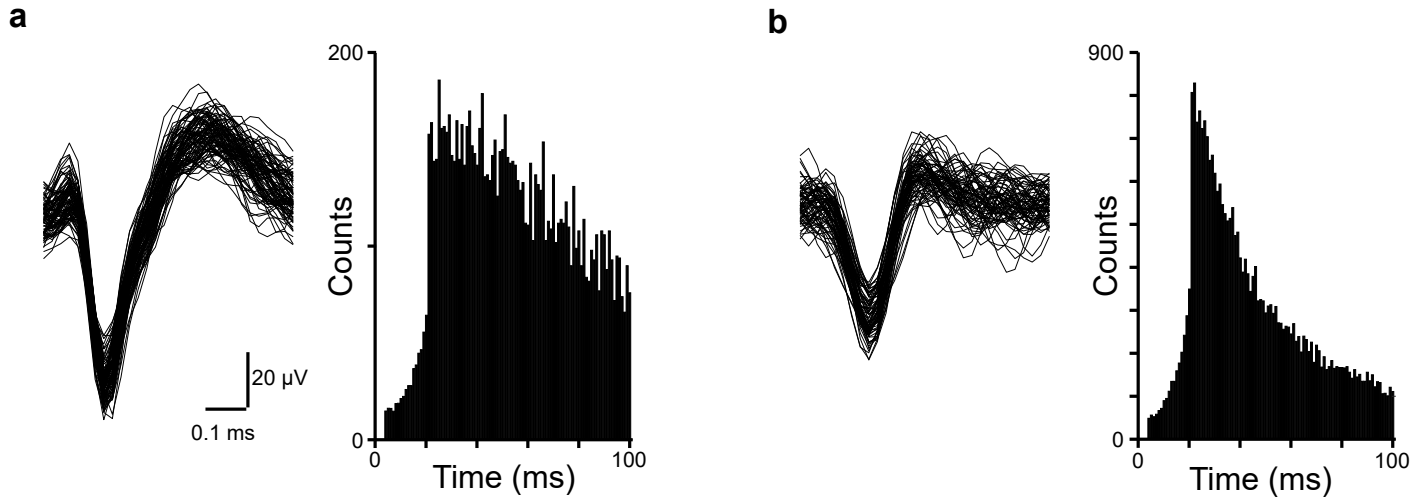
a
20 μV
0.1 ms
200
Counts
0
0
100
Time (ms)
b
900
Counts
0
0
100
Time (ms)

Figure S2

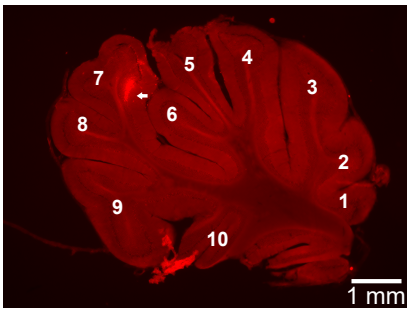

Figure S3

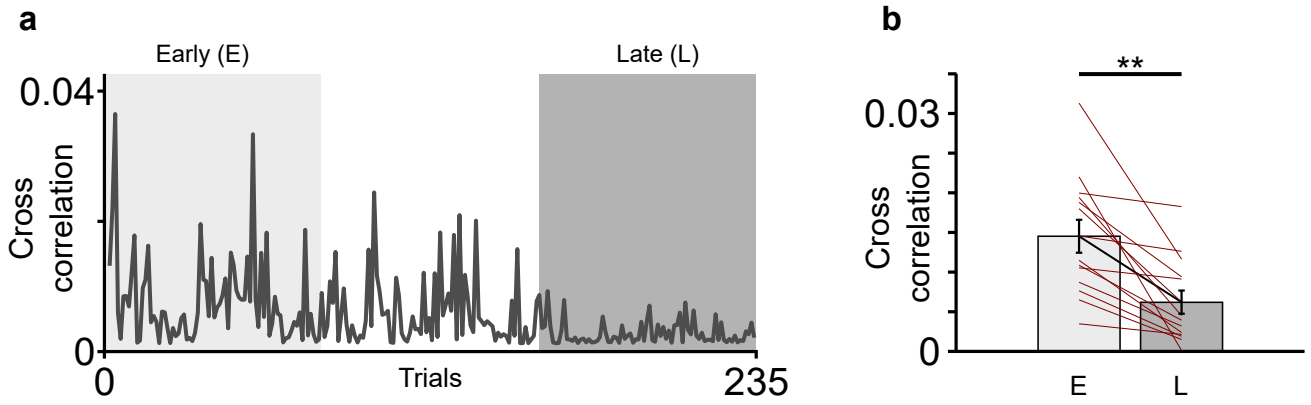
a
Early (E)
Late (L)
0.04
Cross correlation
0
0
Trials
235
b
**
0.03
Cross correlation
0
E
L

Figure S4

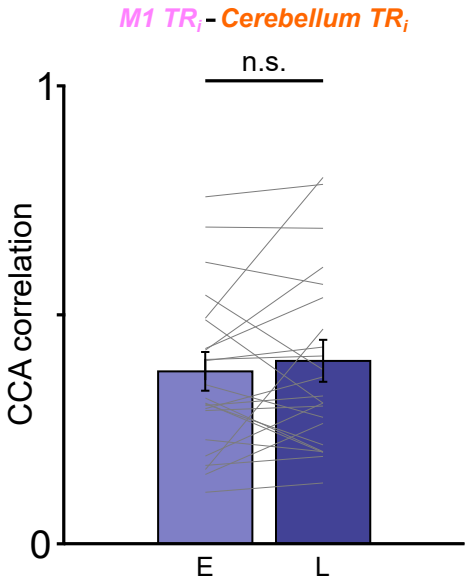

Figure S5

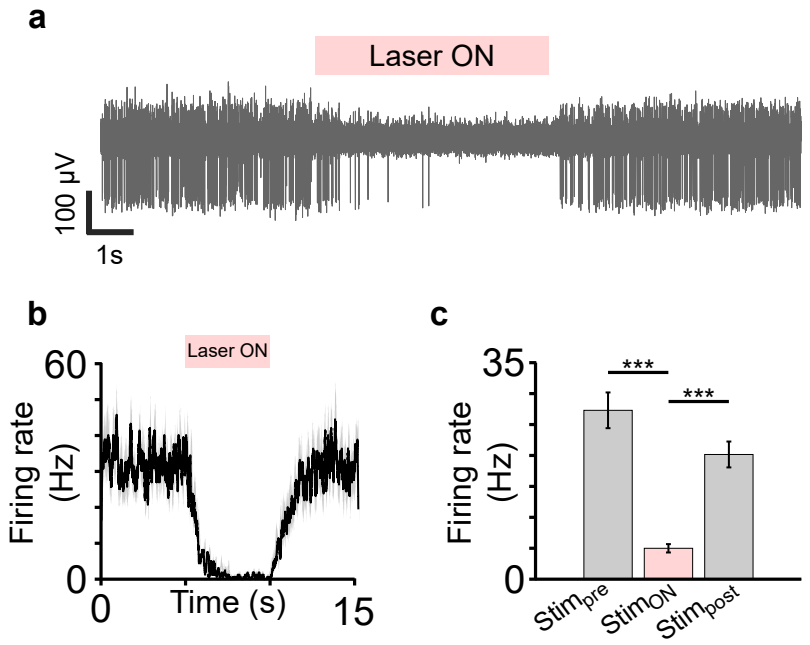
a
Laser ON
100 µV
1s
b
Laser ON
60
Firing rate (Hz)
0
0
Time (s)
15
c
35
***
***
Firing rate (Hz)
0
Stim_pre
Stim_ON
Stim_post

Figure S6

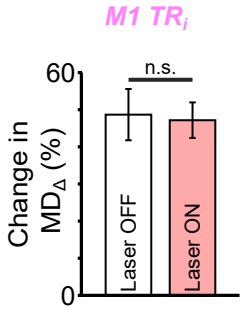

Figure S7

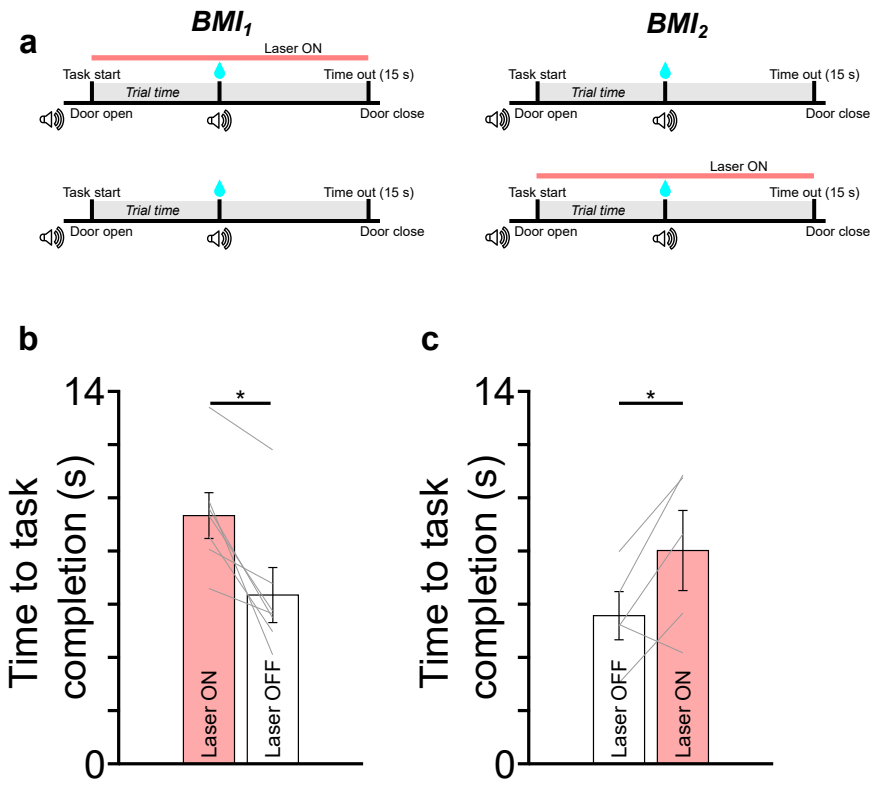
a
BMI1
Laser ON
Task start
Trial time
Time out (15 s)
Door open
Door close
BMI2
Laser ON
b
c
14
0
Time to task completion (s)
*
Laser ON
Laser OFF